UNIVERSITY OF CALIFORNIA SAN DIEGO

A Waveform Generating and EEG Processing System (TX & RX) for Focused Ultrasound Neural Stimulation

A Thesis submitted in partial satisfaction of the requirements

for the degree Master of Science

in

Electrical Engineering

(Medical Devices and Systems)

by

Lu Xu

Committee in charge:

Professor Ramesh Rao, Chair
Professor Mingxiong Huang
Professor Imanuel Ruvin Lerman
Professor Sheng Xu

2019

The Thesis of Lu Xu is approved, and it is acceptable in quality and form for publication on microfilm and electronically:

_____

_____

_____

_____

Chair

University of California San Diego

2019

TABLE OF CONTENTS

LIST OF FIGURES:

LIST OF TABLES:

LIST OF EQUATIONS:

LIST OF SUPPLEMENTAL FILES:

LIST OF ABBREVIATIONS:

CT: Computed Tomography

EEG: Electroencephalogram

EP: Evoked Potential

f_c : Center Frequency

FDA: Food and Drug Administration

FUS: Focused Ultrasound

FUS-NS: Focused Ultrasound Neural Stimulation

GPIO: General Purpose Input-Output

HIFU: High Intensity Focused Ultrasound

KZK: Khokhlov–Zabolotskaya–Kuznetsov

MI: Mechanical Index

PCB: Printed Circuit Board

PCI: Passive Cavitation Imaging

P_{NP}: Peak Negative Pressure

P_{PP}:Peak Positive Pressure

RX: Receive Sub-system

SSEP: Somatosensory Evoked Potential

TTL: Transistor-Transistor Logic

TW: Transmit Waveform

TX: Transmit Sub-system

USEP: Ultrasound Somatosensory Evoked Potential

ACKNOWLEDGEMENTS

I would like to acknowledge Professor Ramesh Rao for his support as the chair of my committee. His guidance has proved invaluable throughout the past two years.

I would also like to acknowledge Dr. Imanuel Lerman for his inspiration and support through the past two years. Dr. Lerman was the one that lead me into the research in medical devices. Without him, I wouldn't be doing this at all.

I would like to express my appreciation to Donald Kimball as he selected me for this lab position two years ago. His support in all engineering related matters contribute greatly in my research throughout my time in this lab.

I would like to thank Rahul Singh and Kristen Nguyen for helping me in finishing Chapter 2 and Chapter 3. Their support has proved invaluable throughout the past two years.

I also would like to thank Professor Sheng Xu and his group for lending us their acoustic tank to me and assisting me in the testing. The corresponding results is included in Chapter 2.5 and Chapter 3.2.

I want to express special appreciation to Yan Gong. Her support, encouragement and caring sustained me daily in my past two years' work and my work towards this thesis.

The schematic of AIMS III acoustic tanks in Figure 19 was taken from its datasheet with the permission from Onda Corp.

Chapter3, section 3.3, in part, is a reprint of the published work titled "*Measurement of Focused Ultrasound Neural Stimulation; Somatosensory Evoked Potential at Two Separate Skin Temperatures"* in Proceedings of the IEEE International Ultrasound Symposium, 2018, Lu Xu, Yan Gong, Donald Kimball, Rahul Singh, Kristen Nguyen, Ramesh Rao, Mingxiong Huang and Imaneul Lerman. The thesis author was the primary investigator and author of the paper.

ABSTRACT OF THE THESIS

A Waveform Generating and EEG Processing System (TX & RX) for Focused Ultrasound Neural Stimulation

by

Lu Xu

Master of Science in Electrical Engineering (Medical Devices and Systems)

University of California San Diego, 2019

Professor Ramesh Rao, Chair

Neural stimulation with focused ultrasound is a rapidly developing research field. This thesis demonstrates design and validation of a comprehensive focused ultrasound neural stimulation (FUS-NS) research system that can both generate ultrasound pulses with user-definable parameters and process the elicited Electroencephalographic (EEG) responses from human test subjects. Several ultrasound transducers were characterized with different methods including both simulation and experimental measurements to ensure safety and confirm parameter space. Parameter sets were swept in acoustic tank and measured with hydrophone before human subject tests to ensure safety. EEG data were analyzed with custom-built MATLAB script to sort and extract user-definable patterns. Different versions of the transmit sub-system (TX) was built and tested and will be presented in this thesis. Our human study showed that FUS-NS system was safe for use in human subjects and activated peripheral neural nociceptors (free nerve endings), and a resultant painful sensation was perceived when the system was tested. The pain sensation was recorded with our EEG evoked potentials (EP). The human subject study (N=3) confirmed safety of the system as well as all the proposed functionalities. This system will greatly

facilitate the research in focused ultrasound neural stimulation. Our laboratory has now moved to characterize additional FUS-NS aimed to stimulate axonal neuronal structures.

Introduction:

Electrical impulses known as action potentials are the logic-gated signals used by neuron cells in the brain and peripheral nervous system to transmit information. Neuronal action potentials result in the release of neurotransmitters, the chemical elements responsible for inter-cellular signaling that drive behavior, learning, memory and motor function. Invasive techniques for peripheral nerve stimulation have been employed in humans for pain management (closed loop spinal cord stimulation), preventing a seizure in epileptic patients (closed loop cortical stimulation), treatment of Parkinson's disease, (closed loop deep brain stimulation) and cardiac dysfunction (closed loop pacemakers). Common to all the current technologies is the fact that invasive neural recording requires surgical intervention fraught with complications related to implant as well as continuous neural inflammation (glial activation) and scarring that occurs with chronic implantation of foreign objects [1]. With surgical implantation of vagus nerve electrodes (capable of stimulating the vagus nerve) there is similar risk for procedural operative complication due to chronic implant that may damage the vagus nerve. It is well documented that long term implantation of electrodes in close approximation to neuronal structures can lead to local inflammatory processes that also can result in damage to the vagus nerve. Therefore, there is a clear need for non-invasive technologies that safely stimulate the vagus nerve without the possibility of imparting chronic neuronal damage. Focused ultrasound neural stimulation (FUS-NS) has the potential to be used as a non-invasive replacement of the conventional procedures that can be used safely. Multiple groups have now demonstrated that focused ultrasound can reliably stimulate peripheral nerves in pre-clinical models, while emerging work in humans has also recently been demonstrated [2]. Our laboratory has moved forward to human studies on the bioeffects of focused ultrasound applied to the peripheral nervous system. To facilitates this research, a safe, reliable, accessible and comprehensive focused ultrasound research system is needed. This thesis describes our design, building and testing of such a FUS-NS system. This system consists of both the transmitting sub-system (TX), which produces acoustic pulses with user-definable parameters, and receiving sub-system (RX), which acquires and analyzes

electroencephalogram (EEG) data from human subjects. The system design included incremental prototypes as the research in this lab developed over time, which will be elaborated in the following sections. First, a single-element focused ultrasound TX sub-system was built with benchtop equipment such as digital function generator and stand-alone power amplifier to achieve basic functionality. Then effort was put into system integration to achieve portability. To prove efficacy and safety of our benchtop ultrasound system, a human subject ultrasound neural stimulation study with a small cohort (N=3) was carried out with the designed system. To be able to stimulate deeper tissue that are potentially surrounded by complexed structures, a multi-element focused ultrasound system was designed and developed that can support interleaved B-mode imaging during stimulation and real-time FUS-NS steering. This thesis systematically describes the incremental development of the FUS-NS TX and RX system in detail.

Chapter 1: Background

1.1 Bioeffects of Ultrasound on tissue:

Ultrasound can produce thermal or mechanical bioeffects on tissue. Thermal bioeffects are due to tissue's absorption of ultrasound's mechanical energy. Heat is produced and deposited in the tissue due to lag between condensation and change of pressure, which can cause temperature increase. Mechanical bioeffects are associated with cavitation. Two main types of cavitation occur during FUS pulsation: stable cavitation and unstable cavitation. Stable cavitation is the oscillatory behavior of gas bubbles within medium while unstable cavitation, or inertial cavitation, expands rapidly in volume and releases large amount of mechanical energy upon its collapse, creating tearing and cavity in the medium. The following sections will further elaborate the background of these bioeffects.

1.2 Thermal Bioeffects:

Absorption of Ultrasound wave in liquid:

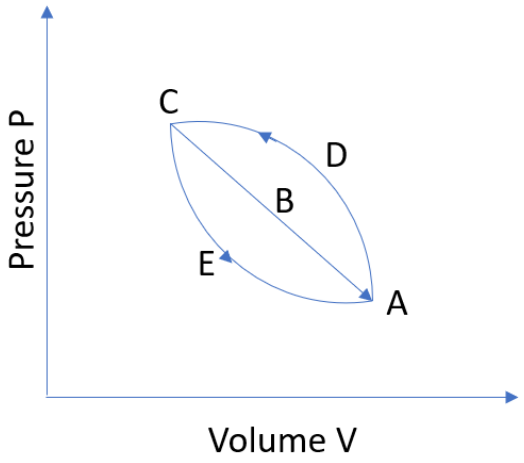

Figure 1: Volume-Pressure plot to illustrate effect of lag between condensation and pressure on net work done to the system.

Absorption of ultrasound wave constitutes the attenuation and temperature elevation in the medium. As a cornerstone to FUS safety we will systematically describe how US energy is dissipated and lost during absorption. Ultrasound is a spatial longitudinal wave. The wave exerts pressure upon medium and changes its local volume during propagation. Counterintuitively, pressure and condensation do not

happen at the same pace in liquids. Viscosity of liquid creates a lag between onset of pressure and change in volume. This lag causes a non-zero net work done by the ultrasound wave to the local medium in the form of heat [3]. Volume-Pressure plot (Figure 1) demonstrates this effect. When condensation and pressure are fully synchronized, pressure and volume follow curve ABC during the positive pressure phase and CBA during negative pressure phase [3]. The work done by the ultrasound wave (W(J)) in respect to pressure (P(Pa)) to the liquid medium follows:

Equation 1:

$$W = -\int_{V1}^{V2} P\, dV$$

The work done during the positive pressure phase will be returned to the medium in the negative pressure phase. Therefore, net work done by the wave to the medium is zero when pressure and condensation are synced in time. However, when condensation lag pressure exertion, pressure and volume follow curve ACD and similarly when under expansion, follows by CEA [3]. By Equation 1, the net work done after one complete cycle of ultrasound wave is the area under shape AECA which results in net heat dissipation. This effect is categorized as the absorption of ultrasound by the medium and leads to temperature elevation in the medium.

1.3 Cavitation Bioeffects

Cavitation refers to a set of behaviors including formation, oscillation and bursting of gas bubbles in the medium under an external pressure field such as ultrasound [3] [4] [5] [6]. The monitoring of cavitation is critical to safe use of FUS-NS as some forms of cavitation (inertial cavitation) can cause mechanical damage to tissue. Cavitation begins with the formation of gas bubbles under the external pressure field. The external pressure field overcomes tensile strength between liquid molecules and the diffusion of gas molecules [3] [6]. If external pressure field has large enough amplitude and duration, the formed bubble will either oscillate (non-inertial cavitation) or burst (inertial cavitation). In most cases non-inertial cavitation refers to the oscillating gas bubbles under small pressure field [4]. Non-inertial

cavitation does not pose high stress over tissue and therefore is referred to as "stable" cavitation [5]. Stable cavitation is generally safe and does not cause chemical or structural changes in the surrounding medium [4]. As magnitude of the pressure field increases, there is relative direct increase in rate of gas bubble volume fluctuation [6]. Increases in pressure field can result in gas bubble collapse, as surrounding fluid fails to keep pace of the expansion of gas bubble due to its inertia. Inertial cavitation is due to the collapses of gas bubbles that then creates shock waves. Shock waves (H(t)) are temporally impulse-like and can be approximated as a very narrow rectangular function with width $\frac{1}{2\tau}$:

Equation 2:

$$H(t) = rect(\frac{t}{\tau})$$

The Fourier transform of Equation 2 yields:

Equation 3:

$$F_{H(t)}(\omega) = \frac{\tau}{2} sinc(\frac{\omega\tau}{2})$$

As shock wave approximates Dirac function, width of $H(t)$ decreases while width of $F_{H(t)}(\omega)$ increases to create a broad-band emission observable in the frequency domain. Broad-band emission has been observed and characterized with shock wave by measuring frequency domain response of shock wave caused by detonating explosives under water the US Navy [7]. Inertial cavitation poses high stress over the surrounding tissue and can cause tissue stress, shear damage including hemorrhage. As a potential safety limitation, the characterization of inertial cavitation is essential. Moreover, in-vivo measurement of inertial cavitation can be monitored during FUS-NS applications.

Mechanical Index (MI) characterizes the focused ultrasound beam's ability to create inertial cavitation due to its peak negative pressure (P_{NP}) and center frequency (f_c).

Equation 1:

$$MI = \frac{P_{NP}}{\sqrt{f_c}}$$

To obtain in-vivo monitoring of cavitation effects we have developed our own Passive Cavitation Imaging (PCI) system. PCI is a very powerful tool for monitoring inertial cavitation during testing. PCI utilizes inertial cavitation's broad-band emission under frequency domain due to its impulse-like temporal behavior during the bursting. Both above methods are used in this study to ensure safety and its implementation and results will be described in section 2.1 and 3.2.1.

1.4 Evoked potential:

An Evoked potential (EP) or evoked response is an electrical potential recorded from the human nervous system following presentation of a stimulus, as distinct from spontaneous potentials as detected by electroencephalography (EEG) [8]. Somatosensory evoked potential (SSEP) consists of different waveforms cascading together that travel through the somatosensory neural pathways [8]. SSEP has been used in numerous clinical settings to help diagnose the location of damage in the somatosensory pathways. SSEP can be elicited by applying mechanical stimulus and electrical shock to the skin, which are known to have thermoreceptors, nociceptors and polymodal receptors. The summative neural signal can be measured after the respective stimuli as an electroencephalographic waveform. Using the 10-20 system, electrodes are placed on the subject's scalp that allows for SSEP recording. Focused ultrasound has been prior shown to illicit measurable SSEP waveform from the human hand [9] [10] [11]. In this study we developed the FUS-NS system with the goal to measure FUS-NS SSEP at two separate dermal skin temperatures (See section 3.3.2).

1.5 Physiological focused ultrasound stimulation, review of literature:

Forty years ago, research carried out by Gavrilov and his colleagues (1977, 1984, 1996) demonstrated that focused short duration ultrasound stimuli of relatively high intensity can induce a variety of somatic thermal or tactile sensations [9] [10] [12] [11]. Inspired by their work, independent

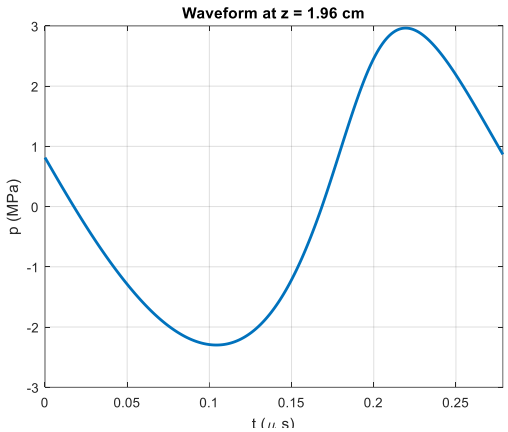

Figure 2: Simulated pressure at target area by HIFU Simulator. Non-ideality feature is shown as asymmetrical positive and negative peaks.

groups started to study the bioeffects of focused ultrasound applied to peripheral nerves. First, Hong et al., (1991) showed focused ultrasound could reversibly block conduction in human peripheral nerves [13]. This result shows focused ultrasound can be used for anesthetic purposes. Foley et al. (2006) showed ultrasound with higher acoustic intensity applied to rabbits' sciatic nerve could block its conduction such that it stopped the motor functions of the corresponding limb [14]. Recently, Downs et.al (2018) achieved motor response from focused ultrasound stimulation to a rat sciatic nerve [15]. All of above successful neurostimulation studies used pulsed waveform of various durations(on times) that likely impart the measured bioeffects, i.e. neuronal inhibition with long on time (5-120 sec) versus stimulation with extremely short (ms) on time and variability in pressure applied. Despite these successful neural inhibition and stimulation cases, the underlying mechanism of FUS-NS is still unknown and hotly debated. As prior work suggests conventional Hodgkin–Huxley modeling of neural conduction, i.e., electro-chemical and not mechanical process are paramount [16], recent work suggests mechanical energy imparted to the axon may result in a soliton which propagates mechanical energy within an axon and may contribute to action potentials propagation [17].

In conclusion, focused ultrasound (FUS) generates both thermal and mechanical bioeffects. FUS has been demonstrated to successfully illicit evoked potential when applied to peripheral neural system

with pulsed waveform. The potential damage caused by heat and cavitation created by FUS needs to be avoided and closely monitored during stimulation.

Chapter 2. Methods

2.1 Safety & Regulation

2.1.1 Thermal:

a. Thermal safety limit:

Focused ultrasound produces heat at the focal spot due to tissue's absorption of the ultrasound energy. Currently there is no specific government regulation over focused ultrasound used as neural simulation therapy. The closest applicable regulation, 21 CFR 1050.10, applies to "physical therapy products," also known as "diathermy product" [18]. Diathermy products are used to generate gentle heat in deep tissue for pain management purposes and is approved to increase deep tissue temperature to 40-45 °C. Beside Diathermy, High Intensity Focused Ultrasound (HIFU) is FDA approved to ablate tissues, including a targeting a cancerous tumor or abnormal vessels [19] [20] [21]. Focused ultrasound for tissue ablation produces and maintains tissue temperature at 55 °C for 1 sec, which is known to cause tissue necrosis [20] [22] [23], The purpose of our program and this study is to perform neuronal stimulation and without tissue damage or ablation; therefore ultrasound waveform must be carefully designed such that the produced heat is well below 55°C.

b. Validation of temperature:

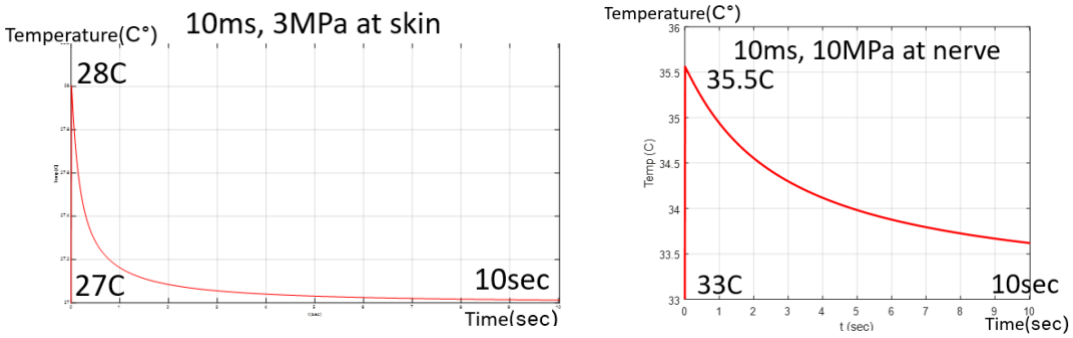

Figure 3: Simulated temperature change at target area by HIFU Simulator. Temperature plot is made by integrating temperature change in each complete waveform cycle.

To design and predict temperature change for different waveforms, I used High Intensity Focused Ultrasound (HIFU) Simulator developed by Food and Drug Administration (FDA) to simulate the heat

produced. With user provided information on transducer geometry, acoustic properties of each layer of tissue along the axis of propagation and ultrasound waveform, HIFU simulator can simulate target pressure waveform with non-ideality features by integrating the asymmetric KZK equation from the frequency-domain. Using simulated pressure distribution profile within tissue, HIFU simulator then runs bioheat transfer equation (BHT) to simulate the additive effects of temperature from each cycle of ultrasound pressure waveform [24]. The simulation was carried out with two base temperatures: 33°C and 15°C. The acoustic propagation path was designed to have two layers: water and human skin tissue. Their corresponding acoustic properties were entered into the simulator [25].

To ensure accuracy of simulated temperature results and safety, we used HIFU Phantom Gel (Onda

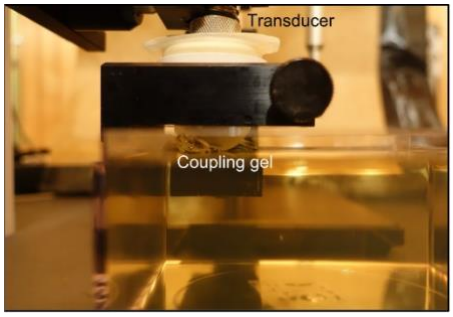

Figure 4: HIFU Phantom Gel used to test whether temperature increase at focal spot would cause tissue damage.

corp.) to test whether temperature increased at focal spot would create thermal damage to tissue. Region inside HIFU Phantom Gel that has temperature close to 70° C will turn opaque.

c. Temperature control during human testing:

With both the HIFU Simulator and HIFU Phantom Gel, we designed a set of ultrasound waveforms that is thermally safe. As mentioned in the Introduction, we carried out a human study to validate the designed system. During the human testing, which will be elaborated in section 3.3.2, skin temperature was measured and monitored with infrared thermometer (LASERGRIP800, ETEKCITY, Anaheim, California, US). Subjects were either exposed to cold or warm temperature on the hand palmar dermal surface. For the warm temperature group, the temperature at ultrasound target is held constant at 26°C

while for cold temperature group, 10 °C. Skin dermal temperature was cooled using ice (measuring 2cm by 2cm encased in waterproof latex bag). Subdermal (below skin surface) region base temperature were estimated using existing model [26]. Details on this human study are elaborated later in section 3.3.2.

2.1.2 Cavitation:

a. Cavitation safety limit:

Mechanical Index was used to determine likelihood of inertial cavitation for each ultrasound waveform based on its peak negative pressure (P_{NP}). According to FDA regulations for diagnostic ultrasound, MI needs to be lower than 1.9 such that inertial cavitation(known to cause tissue damage) is unlikely to occur [27]. According to Equation 4 (MI), both peak pressure and center frequency determine MI. To prevent any inertial cavitation, we developed an ultrasound waveform with a calculated MI that is lower than 1.9.

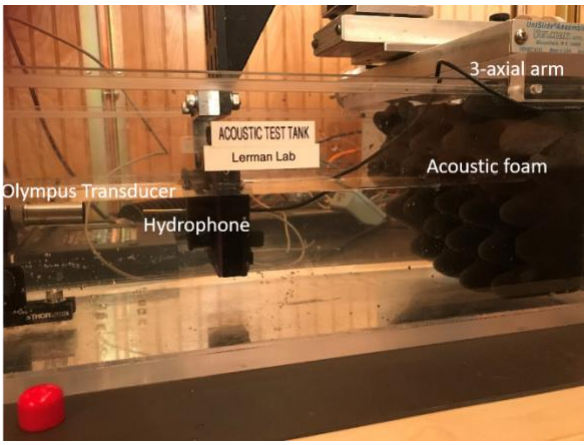

Figure 5: Experiment setup of validation of pressure and hydrophone scan. A large piece of acoustic foam was installed on the far end of beam axis to prevent reflection of acoustic energy.

b. Validation of Pressure:

Peak pressure of the designed waveforms was measured and validated using an HNR-1000 hydrophone (Onda Corp., Sunnyvale, CA). Single element focused ultrasound transducers SU-107 and A382S-Su-F-0.83-IN-PTF (Olympus Corp., Center Valley, PA) were mounted on the bottom of a custom-made acoustic water tank. The HNR-1000 hydrophone was mounted on a 3-axial arm with 0.1mm

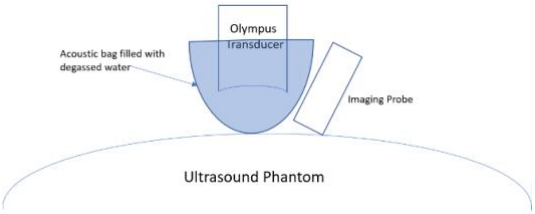

Figure 6: Illustration of PCI setup. Imaging probe was placed aside the HIFU transducer with a tilt angle (Acute) with a tilted angle.

movement accuracy. The position and aim of the hydrophone were carefully tuned such that the location of focal spot overlapped the front membrane surface of the hydrophone. The peak negative pressure (P_{NP}) was then measured across all selected waveforms to calculate MI.

c. Validation of Cavitation:

Passive Cavitation Imaging (PCI) was used to validate absence of inertial cavitation for SU-107 and A382S-Su-F-0.83-IN-PTF. PCI was carried out with a 192-element Imaging transducer (L12-3V) with Vantage 256 system (Verasonics Inc., Kirkland, WA). During PCI acquisition, the Olympus transducer was mounted inside an acoustic invisible bag filled with water, aimed at an ultrasound training phantom (CAE Healthcare, Sarasota, FL). During testing, all transmit channels on L12-3V were turned off to avoid acoustic interference with the Olympus transducer beam. After acquiring the data, the PCI algorithm was used to plot the spatial profile of acoustic intensity at the fundamental, second harmonic and inharmonic frequencies, along with power spectra density (PSD) plot from DC to 10MHz frequency band. Of note that current system does not support PCI with multi-element transducer H-102, as will be elaborated in section 2.2.2.

2.1.3 Characterization of transducer beam:

This system aims to support a range of transducers including single-element transducer A328-Su-F-0.83-IN-PTF, SU107, both running at 3.5MHz, and two versions of the multi-element transducer H-102, one running at 1.1 MHz and the other at 3.5MHz. To verify beam profiles reported by the manufacturer, both 2-D pressure field simulation and tank scan were performed to aforementioned transducers except H-

102 at 3.5MHz, which was not eventually manufactured. The following sections elaborate on 2-D simulation of the above transducers.

a. KWave Simulation:

KWave simulator is an open-source MATLAB based acoustic simulator. It computes pressure field profile in a predefined simulation space by solving the following equation set. When solving these equations, KWave assumes acoustic properties such as sound speed, while the geometries and densities remain the same [28].

The first step of simulation is to create a space in the simulator that contains both the focused ultrasound transducer with its beam. For free-field simulations, this space is filled with water. Then each transducer was modeled in the simulator. For single-element transducers this process is straightforward.

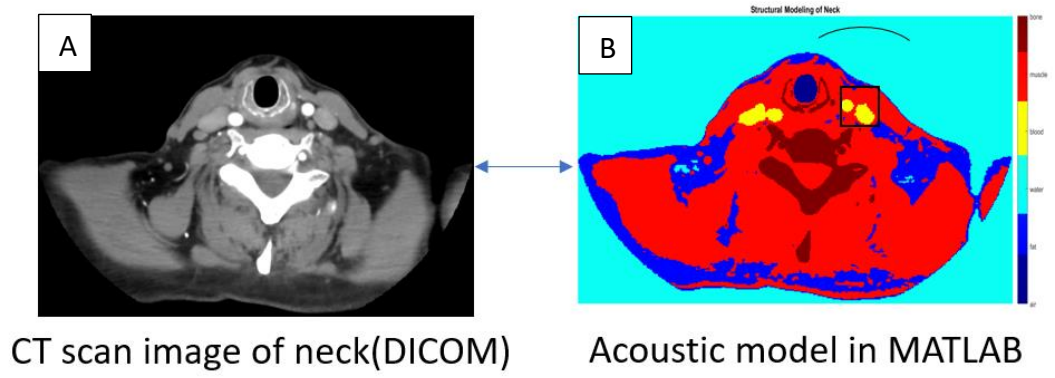

Figure 7: Demonstration on simulation of beam profile inside human body. A: Computed Tomography image of human neck; B: modeling of CT scan image with MATLAB using custom-built script, different types of tissues were sorted by their difference in contrast and shown in different colors. An arc defined as source was used to model the real single-element transducer. The beam was expected to be inside the box.

Equation 5: u: acoustic particle velocity, p: acoustic pressure, ρ: acoustic density, ρ0: ambient (or equilibrium) density, c0: isentropic sound speed.

$$\frac{\partial \mathbf{u}}{\partial t} = -\frac{1}{\rho_0}\nabla p \ , \qquad \text{(momentum conservation)}$$

$$\frac{\partial \rho}{\partial t} = -\rho_0 \nabla \cdot \mathbf{u} \ , \qquad \text{(mass conservation)}$$

$$p = c_0^2 \rho \ . \qquad \text{(pressure-density relation)}$$

The single-element transducer was first modeled as a curved surface in the simulation space. A 2-D slice of the above modeling was taken as the pressure source to perform a 2-D pressure field simulation. This works for single-element transducer due to their geometrical symmetry, which the multi-element transducer lack. Therefore, the entire 3-D modeling of multi-element transducer (especially a random-array such as H-102) has to be used as the pressure source in the 3-D pressure field simulation. To model a multi-element transducer in 3-D, the simulation space needed to be first expanded to 3-D. Then 3-D coordinates of each element were entered the predefined simulation space. 3D shaped "Bowls" with 4mm diameter were created at the aforementioned coordinates to model the ultrasound elements in H-102. The simulator was then readied to move forward to define parameters within the ultrasound propagation medium.

Two main propagation media are supported in this proposed system: free-field and human anatomical structures. Free-field simulation uses water as propagation medium. For this type of simulation, all medium pixels in the simulation space (all pixels except the source) were defined as water. Simulation performed with human anatomical structures requires careful modeling of propagation medium. Human Cervical structure, with more than 4 acoustically different types of tissues and complexed inner structures, was modeled to demonstrate modeling capability of the proposed system and to illustrate the steps of such modeling. The cervical structures of interest (i.e. vagus nerve within the carotid sheath) was visualized via incorporation of a human cervical neck image from a clinical grade Computed Tomography (CT) imaging system. Tissue types in CT images can be easily differentiated by their different contrast values. Then regions of the image were then sorted into types of tissues by their different contrast value and subsequently assigned their individual acoustic properties including sound speed and acoustic impedance. The results of such modeling are demonstrated in Figure 7. With both the defined medium and transducer, the simulator then performed ultrasound propagation simulation by updating pressure field of each medium pixel by approximating solutions for Equation 5.

b. Hydrophone scan:

Single-element focused ultrasound transducer was mounted at the bottom of a custom-made acoustic water tank as shown in Figure 5. The HNR-1000 hydrophone was mounted on a 3-axial arm with 0.1mm movement accuracy. Hydrophone then scanned a 3cm x 3cm x 3cm space around the focal spot of the focused ultrasound transducer to create a beam profile. The corresponding results are shown in section 3.2.1.2. Multi-element focused ultrasound transducer was mounted on a different tank system, which will be elaborated in section 2.5.

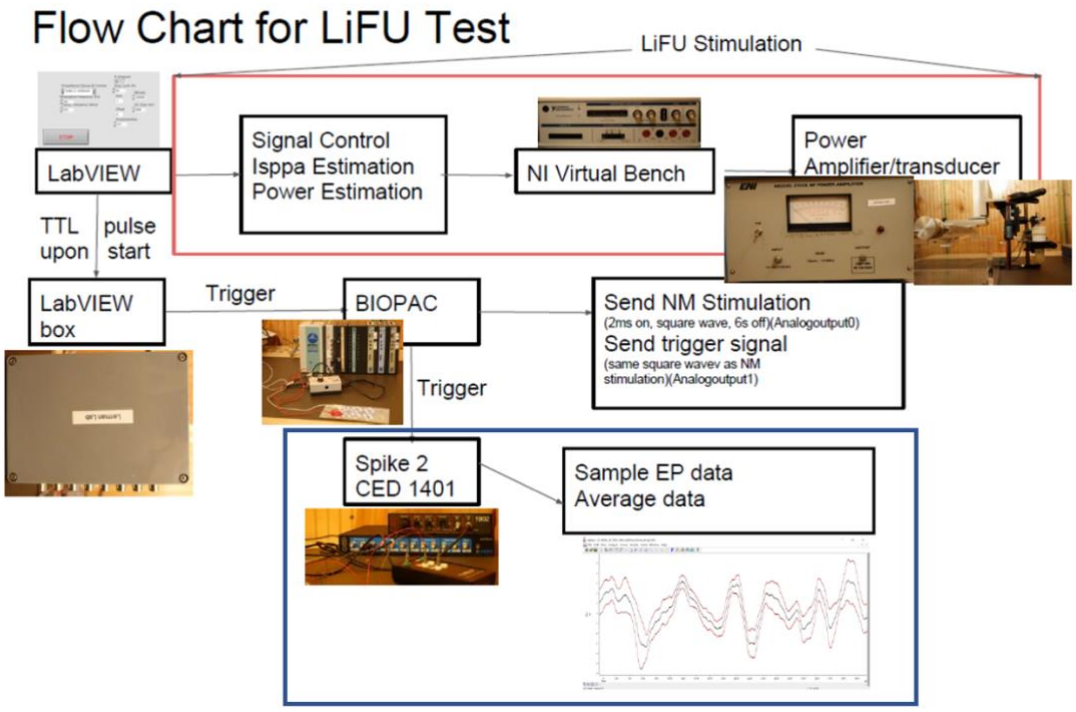

Figure 8: Block diagram of the designed system. TX unit is in red box while RX unit is in the blue box.

2.2 Single-element System Design:

This section demonstrates design of the single element focused ultrasound system. This system is capable of both delivering ultrasound energy to the target and acquiring an evoked potential (EP), importantly with pattern recognition capability. The prototype system was built with bench-top equipment to achieve proposed functionality. Then an improved system that integrated all bench-top equipment except power amplifier was combined into a single printed circuit board (PCB). Both versions of the system consist of two interconnected sub-systems: Transmit (TX) unit and Receive (RX) unit. The TX

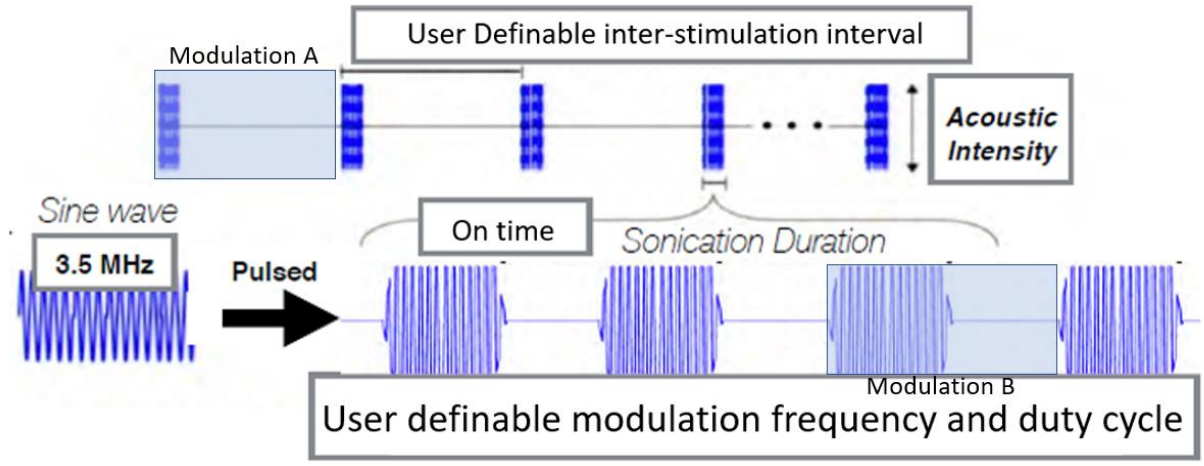

Figure 9: Illustration of each user definable parameters on the generated waveform. Waveform consists of two layers of modulation, modulation A and B. Modulation B is the smaller scale modulation, whose typical period is 30 Hz to 1000Hz; modulation A is the larger scale modulation, whose typical period is lower than 1Hz.

unit handles generation and amplification of the user-designed ultrasound waveform while the RX unit handles acquisition and analysis of the EP.

2.2.1 Transmit Waveform (TW):

Desired transmit waveform (TW) is a double modulated sinewave with a uniform amplitude. The center frequency of the focused ultrasound transducer sets the center frequency of TW, which in this specific case is 3.5 MHz. TW can be modulated by a shorter square wave (Modulation B) and a longer square wave (Modulation A). The on period for modulation A will be referred as "sonication duration" and its off period as "inter-stimulation interval." The on period for modulation B will be referred as "on time." Modulation A has a frequency less than 1 Hz and modulation B has a frequency above 50 Hz.

2.2.2 Passive Cavitation Imaging (PCI)

Passive Cavitation Imaging (PCI) was performed on HIFU transducer SU-107, A382S-Su-F-0.83-IN-PTF with imaging probe IP-105 to monitor level of cavitation that characterized their beam profiles. Passive cavitation imaging beamforms the acoustic waveforms received by each channel on the IP-105 with the conventional B-mode delay-and-sum algorithm.

Distances from each element to the focal point were estimated. The received waveforms were then individually delayed based on the distances between their corresponding channels to the focal point. The waveforms underwent Fourier Transform, that were then squared and integrated over frequency to be converted from pressure to energy over a band of frequencies. By doing the above, PCI plots acoustic energy distribution over space for any harmonically related frequency bands to the transducer's center frequency, which generally includes plots of acoustic energy at fundamental, 2nd harmonic, inharmonic and ultra-harmonic to the fundamental frequency. The plots at fundamental, inharmonic and ultra-harmonic frequencies provide visualization to the beam profile, and most importantly provide estimates of stable cavitation and inertial cavitation [29].

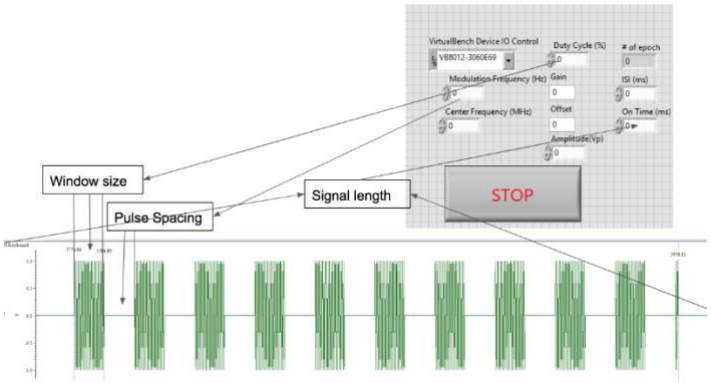

Figure 10: Illustration of user interface of custom-built LabVIEW with the generated modulation B waveform. Waveform shown above is within one sonication duration. Waveform produced by custom-built LabVIEW program and captured with CED 1401.

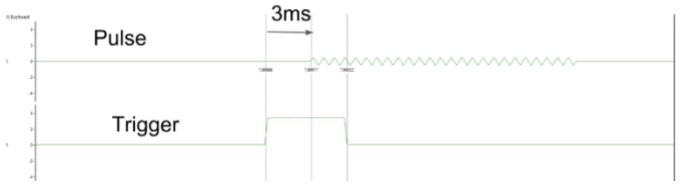

Figure 11: Illustration of trigger signal (bottom waveform) produced by custom-built LabVIEW program at each onset of sonication duration (top waveform).

PCI was implemented on the Vantage-256 system with the IP-105 used as an imaging probe. 'SetUpIP105Flash.mat' was used with all transmit channels turned-off to perform PCI. This was done by setting 'TX' structure to 0 in the 'Event' sequence in 'SetUpIP105Flash.mat'. All data were processed

with sampled code previously published by Haworth et al., (2018) with custom modifications to fit with data output from Vantage-256 with an Nvidia GTX1070 GPU [29]. All acoustic energy plots were normalized in respect to the fundamental frequency. All PCI test were performed in Trainer Branched 4 Vessel phantom (CAE Healthcare, Sarasota, FL) to mimic real human tissue.

2.3 Focused Ultrasound Transmit Unit (FUS TX):

2.3.1 Benchtop TX unit:

The first TX unit incorporated the bench-top function generator (Virtualbench, National Ins., Austin, TX) and custom-built LabVIEW program (National Ins., Austin, TX) running on a local PC to generate analog waveforms. The LabVIEW program collected the waveform parameters with its user to produce discrete samples of desired waveforms. Then the function generator reconstructed the desired waveform from these samples.

The generation of waveform involves trading off between sampling rate and available memory space. According to Nyquist-Shannon's Sampling Theorem, sampling frequency at minimum needs to be twice as large as the sampled signal [30]. Derived from the sampling theorem, waveforms with a set of aliased frequencies are created during reconstruction process. If the sampling frequency is higher than the farther these aliased waveforms are apart from each other on the frequency domain and thus less impactful to the desired waveform [31]. Also, larger number of sample points decrease the amplitude in harmonics as they help the generator output a better sinewave. Therefore, LabVIEW was set to generate 20 samples/period to minimize impact of aliasing and harmonics of the waveform. This resolution required much more memory space than what current Virtualbench programming allowed. Therefore, to allow adequate Virtualbench use a compromise was made to the resolution to minimize number of samples generated, to 10 samples/period. This enabled the Virtualbench to generate samples enough for a 28 ms long waveform which is roughly the period of a 35 Hz square wave and long enough for modulation B. Modulation B was generated by multiplying a square wave with user definable duty cycle and frequency to a continuous sinewave. This generation sequence was looped until reaching one sonication duration. The generator was

then turned off by the program until the onset of next sonication duration. The aliasing noise introduced by under sampling was eliminated by the Olympus transducer A328-SU-F-0.83-IN-PTF. Olympus transducer A328-SU-F-0.83-IN-PTF has a narrow bandwidth of 1.77MHz, with pass band 2.71 – 4.48 MHz, and can suppress alias and harmonics caused by digitization of the transmitted waveform. This filtering output only has the frequency component of the fundamental frequency band, which then translated into the good fit sinewave in time domain.

The LabVIEW program also produces trigger signal (TTL) to the FUS RX unit to mark onset of each sonication duration on the acquired EP data. The FUS RX unit used received trigger signal (TTL) to segment acquired EP data into epochs, which will be shown in detail in the next section. The results of generation of both transmitted waveform and trigger signal are demonstrated in section 3.2.2.

2.3.2 Electrical Stimulation unit:

BIOPAC (utilizing the STMISOC) with additional STM100C module was used to generate controlable eletrical stimulus to the human subjects median nerve. The referenced electrical median nerve EEG/EP response was compared to the FUS-NS of the dermal palm surface, (also within the distribution of the median nerve). STMISOC was used to both cut off output currents and amplify the output voltage. STM100C was used to output a ramp signal to the STMISOC module, which then differentiated the ramp signal to produce a pulse. The voltage gain was therefore controlled by both the slope of the STM100C output and voltage gain knob on STMISOC that ensured adequate median nerve stimulation.

2.4 Focused ultrasound EEG measurement unit (FUS RX)

2.4.1 EEG acquisition unit:

FUS RX unit measures and records EEG signals in response to the ultrasound stimulus, which is referred to as evoked potential (EP). EEG signals have amplitude in the range of 10 - 100 uV and frequency content from around 1 - 50 Hz with a reference point in the posterior auricular area (behind earlobe on mastoid bone). A differential amplifier with large gain at a frequency range 1 – 50Hz was

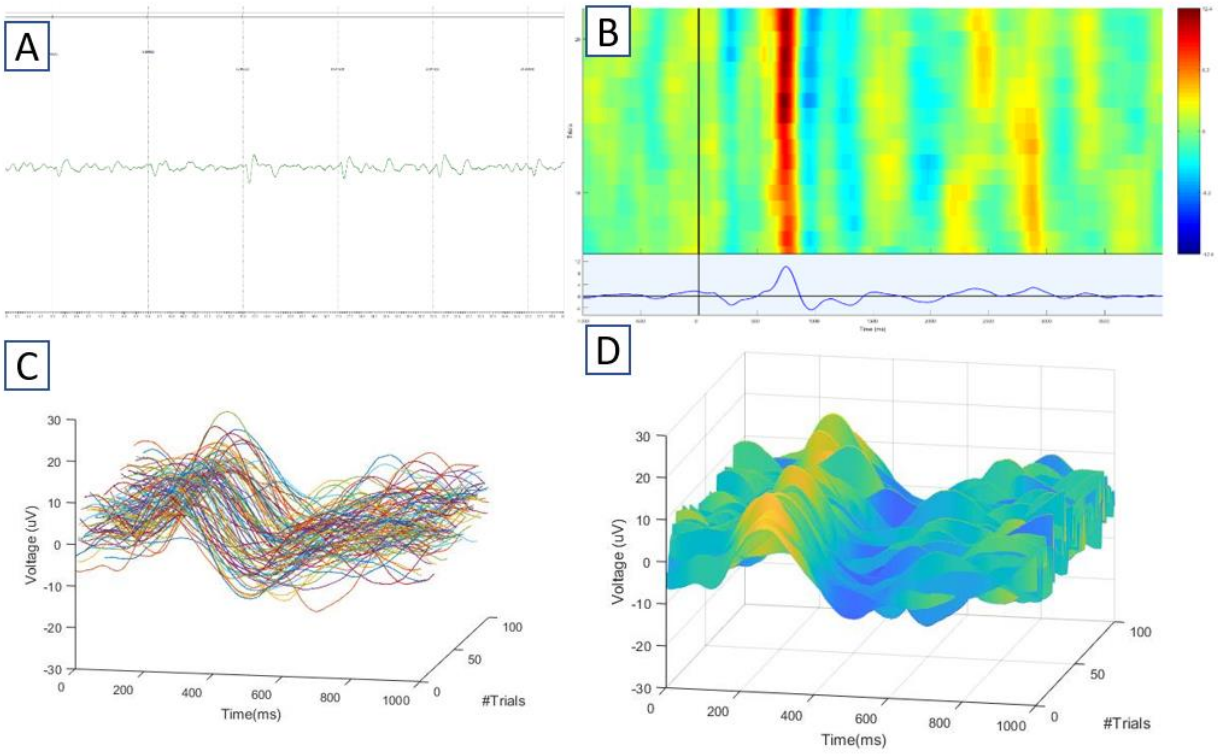

Figure 12: Acquired continuous raw EP data with FUS RX unit. Time stamp marks onsets of each sonication duration(A). ERP plots made from folding 3-D surface plots using FUS RX unit. Vertical line marks onsets of stimulus(B). Raw EEG data partitioned into epochs (C) and then rendered into a surface plot (D).

required. Unlike other conventional electrical reference points, voltage on the human body shifts in response to static charge, heartbeat rhythms and external neural stimulation. Therefore, an amplifier in FUS RX system must be 'right leg driven', or in other word, use the dynamic DC voltage on human body as reference. To accommodate the above requirements, CED 1902 medical EEG amplifier and 1401 data acquisition interface (Cambridge Electronics Design Limited, 139 Cambridge Road, Milton, Cambridge BC24 6AZ, England) were used for this system. Relevant specifics of CED 1902 include 10 GΩ input impedance, input referred noise of 0.3 uV at 1 Hz - 10 kHz for good SNR, CMRR 100 dB (+/ 1V), gain from 60 - 120 dB as well as a bandwidth from DC - 10kHz. Programmable digital filtering provided programmable 2nd or 3rd order Butterworth or Bessel filters. The high pass cutoff ranges from 10 MHz to 1 kHz and the low pass cutoff has a programmable range from 1 Hz - 10 kHz. The ADC in CED 1401 has a 3MHz sampling rate with 16-bit resolution. Data was recorded and streamed over USB to the computer running custom-built data analysis tools.

The toolset for data analysis was designed to sort continuous-time EEG data into epochs. The partition process was done with respect to onsets of sonication durations. The epochs were then visualized on a 3-D plot. Event Related Potential plots of epoch-sorted EEG data were created by plotting the top views of the 3-D plots with color scale.

2.4.2 Pattern recognition unit:

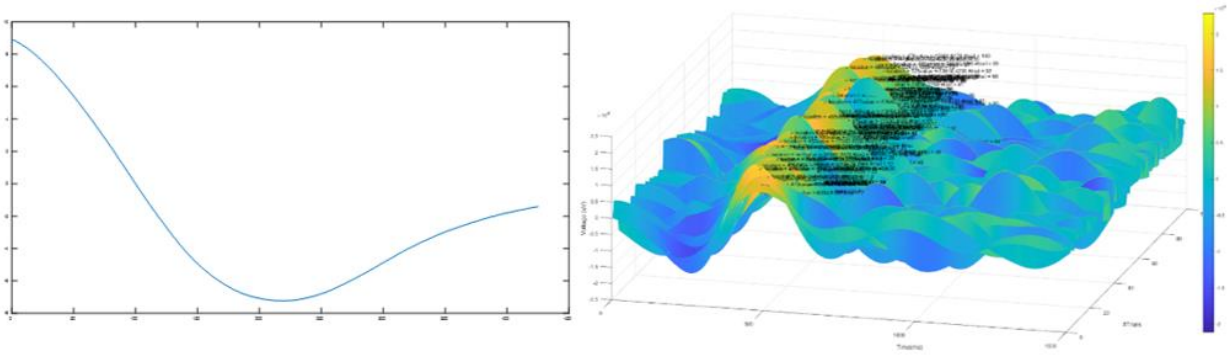

Figure 13: 3-D plot of c(t) (right) with respect to epoch time and #epochs (trials) with pattern of interest (left). Note that c(t) is unitless. Higher c(t) means higher similarity between pattern of interest and EEG data at the corresponding locations.

The FUS RX also offers pattern recognition capability. This is often desirable since researchers are interested in finding out the repeatability of certain post-stimulus EEG responses across hundreds of stimulation trials. This was done in FUS RX using cross-correlation algorithms. The script first takes in a segment of user-defined EEG data, the pattern of interest, and runs cross-correlation with all epochs. Cross-correlation is done by convolving flipped pattern of interest with each epoch. Then the script plots the results of cross-correlation (c(t)) on a 3-D plot and labels their local maxima. Cross-correlation computes similarity between dataset and pattern of interest. Therefore, the locations of each c(t) maxima

Equation 6: Cross-correlation between data $\chi(t)$et and pattern of interest$(\chi_m(t)$ with respect to relative time in each epoch (t).

$$c(t) = x(t) * x_m(-t) = \sum_{\tau \epsilon T} x(\tau) x_m(\tau - t)$$

imply those of pattern of interest within each epoch. With the help of the pattern recognition capability, several signature peaks (P1, N1, P2) and their relative latencies were extracted and compared across epochs.

2.4.2 Source localization of FUS stimulation

Figure 14: Magnetoencephalography set up with Dr. Lerman sitting in. The transducer was enclosed with cardboard covered by steel foil.

To determine the source of FUS stimulation EEG, we used Magnetoencephalography (MEG) to scan our PI, Dr. Imanuel Lerman's brain while subsequently applying electrical and FUS stimulus on his left palmar area. Since MEG is very sensitive to electro-magnetic fluctuations in the environment, all cables and electrodes were carefully shielded with steel braid and FUS-NS transducer was covered with Mu Metal (Manchester, New Hampshire) .

2.5 Multi-element system design

Figure 15: H-102 and cup-shaped mount mounted onto the aluminum frame. Hydrophone was mounted at the bottom of the fish tank.

The Multi-element system provides real-time ultrasound imaging guidance during therapeutic stimulation. Vantage 256 (Verasonics Inc., Kirkland, WA) was used to drive both custom-designed 64-

element high intensity focused ultrasound (HIFU) random array H-102 and IP-105 imaging probe (Sonic Concepts Inc., Bothell, WA). The HIFU random array H-102 was designed to have a central opening of 28.7mm for housing of IP-105. This was done to enable co-axial ultrasound imaging. H-102 was designed to have an operating frequency at 1.1 MHz, focal depth at 51.29 mm and a focal width of 1.31 mm. H-102 is capable of electronically steering the FUS beam(to avoid repetitive stimulation of the same neuronal site), and has a lateral steering range of 13mm and a vertical steering range of 11.9mm. The following sections will demonstrate preliminary verifications done for the multi-element system.

2.5.1 Characterization of H-102 HIFU random array:

2.5.1.1 KWave Simulation:

Like the single-element system, the beam profile of the H-102 was simulated using KWave. All elements were first modeled as a disc with 4.5 mm wide diameter on the surface of the 3D bowl inside the KWave grid. Each element location was determined by the element coordinates provided by the manufacturer, Sonic Concepts Inc. Unlike simulation for single-element transducer, H-102's elements are geometrically asymmetrical. Therefore, 3D simulation instead of 2D was necessary. In this case, 350 layers of 2D simulation were cascaded onto each other to construct the 3D simulation required. In the end, 350 slices of pressure field were generated from the simulation.

2.5.1.2 Tank test:

A tank test was also carried out to verify the beam profile both simulated and reported by the manufacturer. The first tank test was performed in a 10-gallon glass tank (Aqueon Products, Franklin, WI) to verify basic functionality of the multi-element system. The glass tank was filled with distilled water. An aluminum frame was made above the glass tank to mount the H-102 transducer. A hydrophone

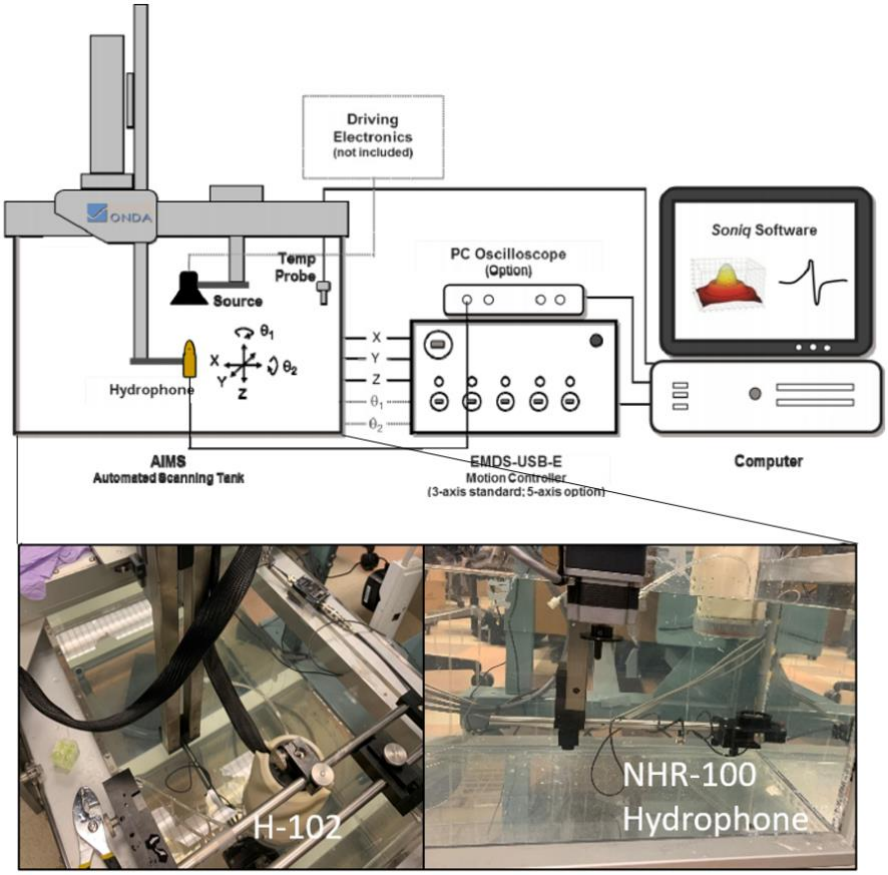

Figure 16: System demonstration of acoustic testing tank used to scan H-102's beam profile. H-102 transducer was mounted with the cup-shaped holder onto the AIMS tank. NHR-100 hydrophone was mounted on the robot arm with an optic coupler from Thorlabs

was mounted at the bottom of the glass tank to coincide with the Z-axis beam propagated from the H102. The H-102 transducer was put into a custom-built cup-shaped holder which was then mounted on the aluminum frame. Position and tilt angle of H-102 were tuned such that the focus beam spot was localized to the front face of hydrophone. The hydrophone readings were displayed using Virtualbench (National Instrument, Austin, TX).

We custom-made a control script on MATLAB to drive H-102 for this tank test. The Vantage system was programmed to send a 500 us sine wave at 1.1 MHz into the H-102. Per channel and overall power output were estimated and kept below safety limit to prevent damage to the H-102 transducer or the hydrophone. Beam steering was achieved by updating delay profile of elements for each bursting. The hydrophone was first placed at the natural focal spot and then moved with the beam when steering was applied.

After the preliminary tank test, beam profile was then scanned with acoustic intensity measurement system AIMS (Onda Corp., Sunnyvale, CA). AIMS provides plot of pressure field by moving the hydrophone across the defined region with a robotic arm. The hydrophone was mounted to the robot arm with an optic coupler (Thorlabs, Inc., Newton, NJ). H-102 was mounted with its cup-shaped holder above the hydrophone to the rod across the AIMS tank. H-102 and hydrophone were carefully aligned to ensure accuracy of the scan. The scan was then performed by the Soniq Software embedded in the AIMS system. The data was processed with Soniq Software and plotted with MATLAB.

2.5.1.3 Interleaved ultrasound HIFU pulsing with user-definable modulation settings and B-mode imaging:

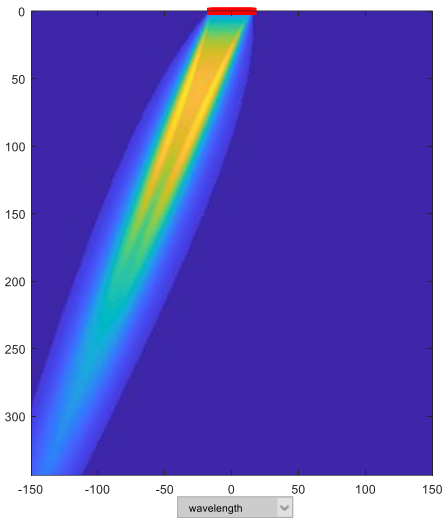

Figure 17: IP-105 beam steered to $-\frac{\pi}{8}$ during the process of creating single frame of B-mode imaging.

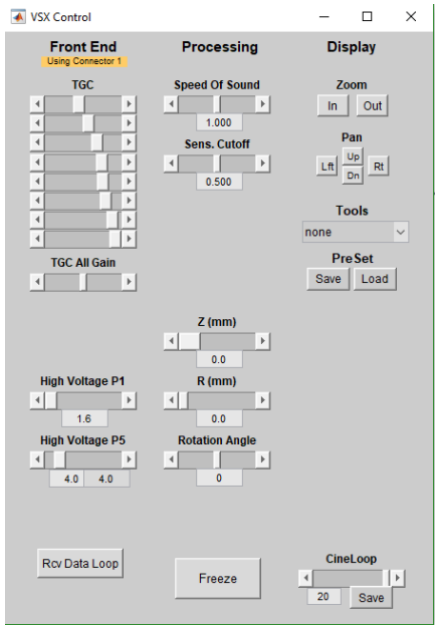

Figure 18: User interface of interleaved imaging and HIFU pulsing. High Voltage P1 controls voltage into IP-105 and High Voltage P5 controls voltage into H-102. Z(mm), R(mm) and Rotation Angle controls vertical, lateral and rotational steering of H-102.

A control script was built for our Vantage-256 system to modulate HIFU waveform and to add B-mode imaging guidance to HIFU therapy based on existing example code provided by Verasonics Inc. The imaging transducer in use for this script was IP-105 (Sonic Concepts Inc., Bothell, WA) and HIFU

transducer used was H-102 (Sonic Concepts Inc., Bothell, WA). Declarations of the two transducers IP-105 and H-102 were carefully laid out in the script for Vantage to properly and safely drive them. The declaration included 3-D coordinates of each ultrasound element and its one-to-one mapping with the Vantage transmitter to enable steering of beams for both IP-105 and H-102. IP-105's beam was steered to scan through the space $(-\frac{\pi}{8}, \frac{\pi}{8})$ around its axial center to create one frame of B-mode image. Steering capability was achieved through changing the delay profile of each transmit channel while the waveforms fed into each channel were the same. The sequence of imaging and HIFU pulsing was controlled by the "Event" structure in the Vantage system. Additionally, the modulation of HIFU waveform was achieved through Verasonics Arbitrary Waveform toolbox (Verasonics Inc., Kirkland, WA).

The schematic of AIMS III acoustic tanks in Figure 16 was taken from its datasheet with the permission from Onda Corp.

Chapter 3. Results:

3.1 Simulation results:

3.1.1 1-D simulation results (HIFU Simulator)

a. Pressure field simulation

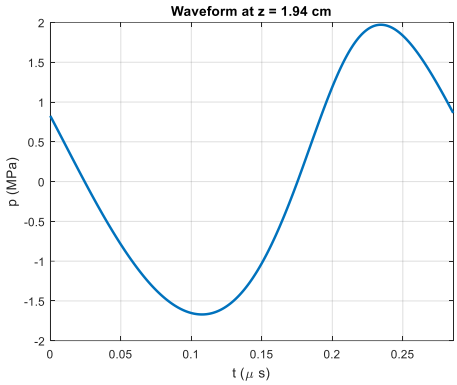

Figure 19: Pressure field at target generated by the HIFU Simulator with interface of water and skin.

Pressure field simulation of Olympus A382S-Su-F-0.83-IN-PTF transducer with HIFU Simulator confirms minimum attenuation occurs as the ultrasound wave travels through 3mm skin tissue. The pressure field simulation results (Figure 19) were used to generate heat simulation results shown in Figure 20. The simulated peak positive and negative pressure results matched with our eventual acoustic tank measurement results with hydrophone (see section 3.1.2).

b. Heat simulation results:

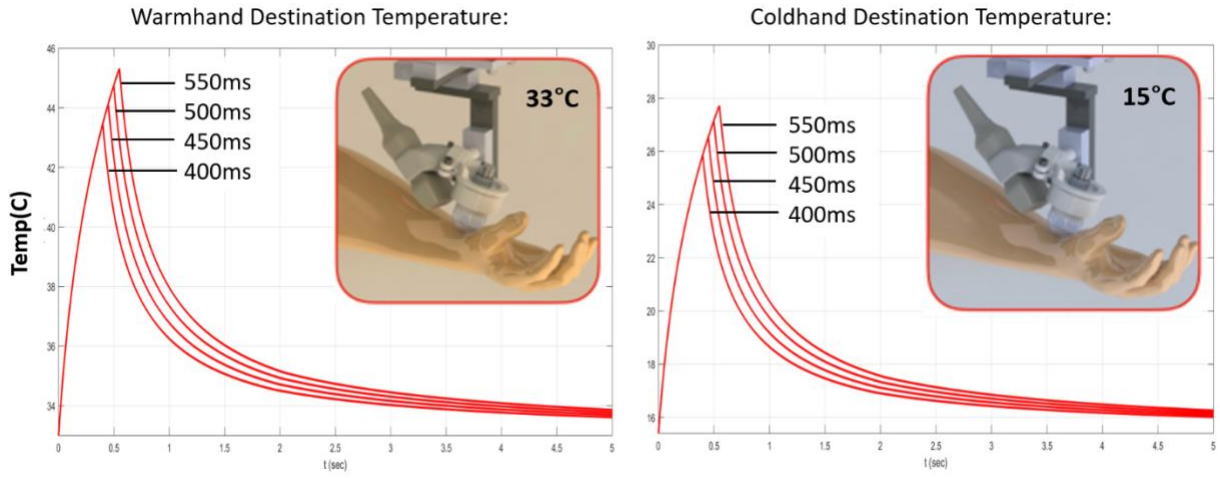

Figure 20: Baseline temperature for warm-hand is 33C°, and destination temperature is 43.45C° (400ms), 44.13C° (450ms), 44.74C° (500ms) and 45.32C° (550ms); (d) baseline temperature for cold-hand is 15.4C°, and destination temperature is 25.85C° (400ms), 26.53C° (450ms), 27.14C° (500ms) and 27.72C° (550ms).

The HIFU heat simulator was used to estimate increases in subdermal tissue temperature introduced by FUS at ambient temperatures(33°C) and with cooled skin(15.4°C). At ambient temperature 33°C and pulse duration from 400 and 450msec, HIFU simulation demonstrates temperature increased from 33°C(base temperature) to 44.5°C, while pulse duration of 500 and 550msec increase from 33°C to 46.5°C. Based on external skin surface and subdermal human skin temperature provided by Saxena et al.,(1983) ice cooling applied to external skin that results in an external skin temperature of 12.4°C translates to a subdermal skin tissue temperature of 15.4°C [32]. HIFU heat simulation from ice cooled base temperature (subdermal tissue at 15.4°C) demonstrates that with 550 ms pulse duration subdermal tissue temperature rose to 29°C. Of note at 29°C heat mediated evoked potential responses do not occur [33], and therefore we postulate the evoked potential recorded at 29°C indeed was exclusively due to mechanical effects of FUS-NS and not due to heat effects.

3.1.2 2-D simulation results (KWave)

a. Pressure field simulation (free field):

Table 1: Summary of reported and simulated beam dimensions of transducers related to this study. The beam dimensions of A328-Su-F-0.83-IN-PTF and SU-107 were measured with HNR-1000 hydrophone with 0.5mm step. The beam dimension of H-102 @1.1MHz was measured with AIMS-III acoustic tank with 0.33mm step on lateral direction and 1mm step on vertical direction.

Transducer	Reported beam width(mm)	Beam length(mm)	Simulated beam width (mm)	beam length (mm)	Measured beam width(mm)	beam length (mm)
A328-Su-F-0.83-IN-PTF	0.7	2	0.83	2	1	2
SU-107	0.46	3.75	0.46	4	0.6	3
H-102 @3.5M	1	2	0.8	2	NA	NA
H-102 @1.1M	3	9.7	2.7	8.89	2	10

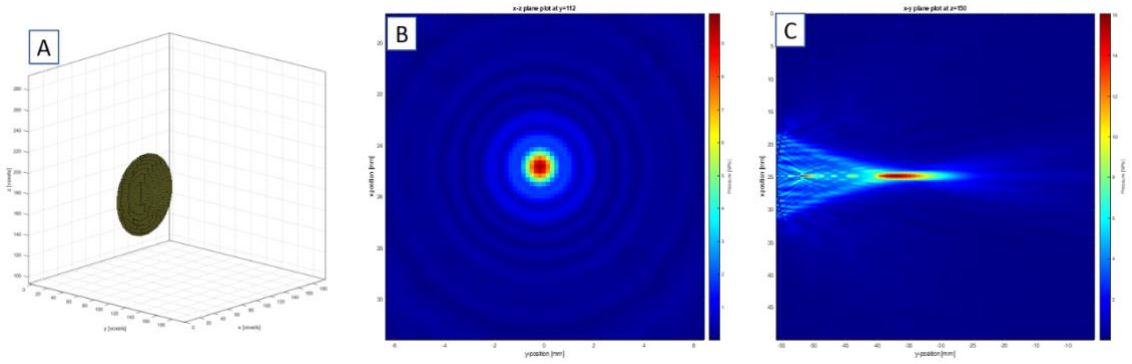

Figure 21: Simulation of A328-Su-F-0.83-IN-PTF. A: modeling of A328-Su-F-0.83-IN-PTF in the simulation space; B: x-z plane cross section of beam profile; C: x-y plane cross section of beam profile.

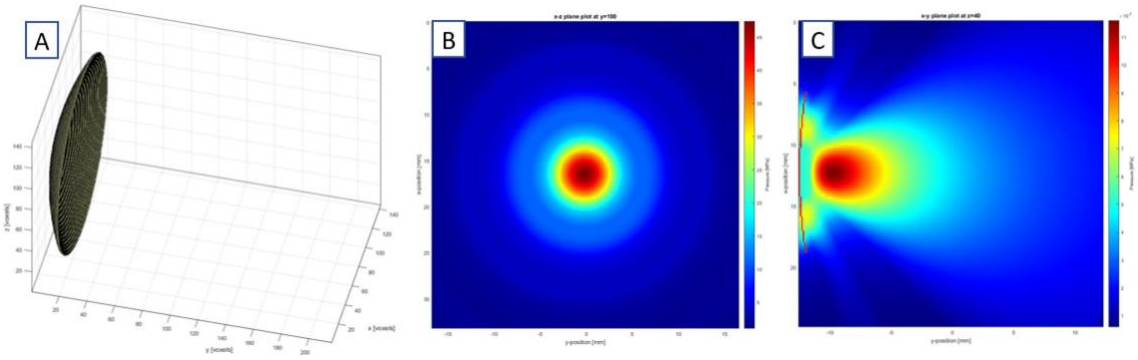

Figure 22: Simulation of SU-107. A: modeling of SU-107 in the simulation space; B: x-z plane cross section of beam profile; C: x-y plane cross section of beam profile.

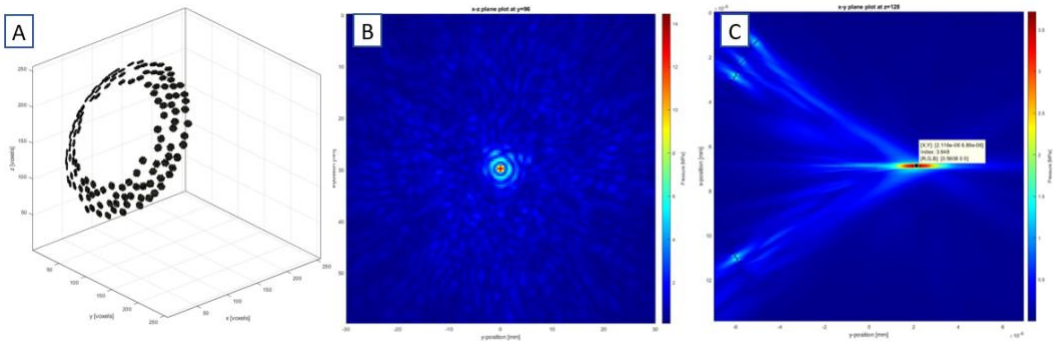

Figure 23: Simulation of H-102 @3.5MHz. A: modeling of H-102 in the simulation space; B: x-z plane cross section of beam profile; C: x-y plane cross section of beam profile.

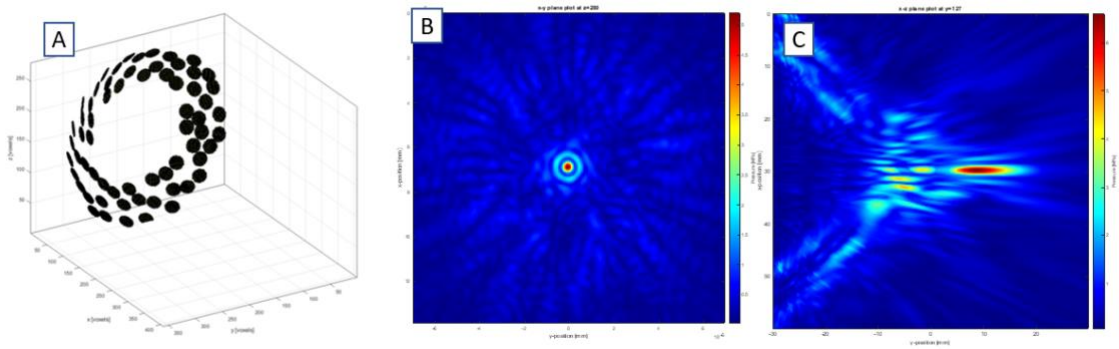

Figure 24: Simulation of H-102 @1.1MHz. A: modeling of H-102 in the simulation space; B: x-z plane cross section of beam profile; C: x-y plane cross section of beam profile.

Free-field simulation results on A328-Su-F-0.83-IN-PTF, SU-107 and H-102 were compared with the manufacturer reported beam profiles, as shown in Table 1, and were found to be very similar to the reported beam profiles. The beam profile of the single-element transducers can be seen in Figure 21

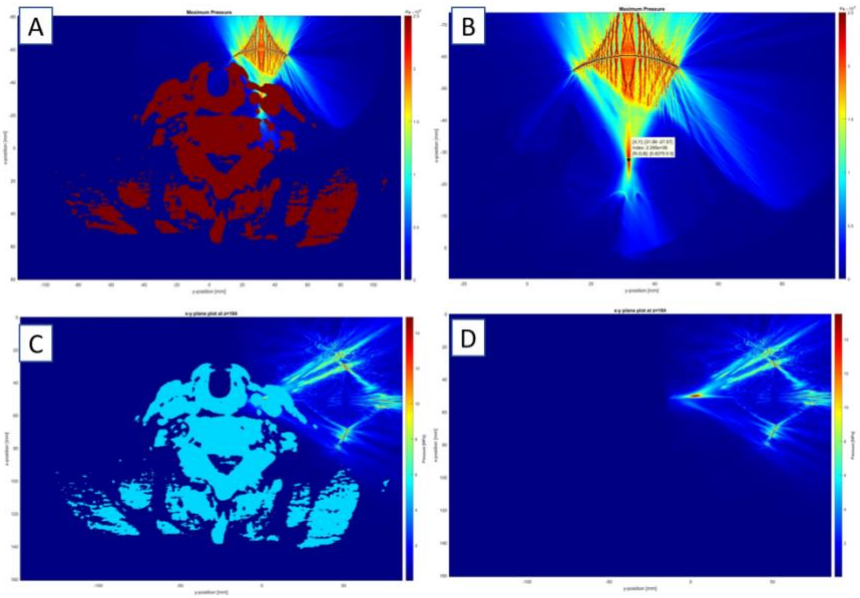

Figure 25: 2-D simulation results of SU-107 through neck targeting at vagus nerve, with mask (A), and without mask (B); 3-D simulation results of H-102 @3.5MHz through neck targeting at vagus nerve, with mask (C), and without mask (D).

and 22. Free-field simulations of H-102 at both 3.5MHz and 1.1MHz were performed during our design process of the transducer, whose results are shown in Figure 23 and 24. Note that although the two H-102 transducers share the same name, their element geometry is very different with each other and hence requires separate simulation. At the beginning we wanted to use this system to stimulate axonal nerves such as vagus nerve and the simulation result shown in Figure 23 show that beam width of 128 element transducer H-102 at 3.5MHz is too narrow to cover the entirety of all axonal fibers within the vagus nerve. Therefore, we modulated the transducer element size and number to the 64 element H-102 at 1.1 MHz. Sampling frequency were 2.07 points/wavelength for A328-Su-F-0.83-IN-PTF, SU-107 and H-102 @ 3.5MHz and 6.6points/wavelength for H-102 @1.1MHz. The simulation results were accurate for all transducers as we compared our simulation beam characteristics to the hydrophone tank test derived measurements.

b. Pressure and heat free-field simulation (in human neck):

Simulation results of both SU-107 and H-102 showed large amount of attenuation at the skin interface. They also demonstrate how the angle of attack can change target pressure. For H-102

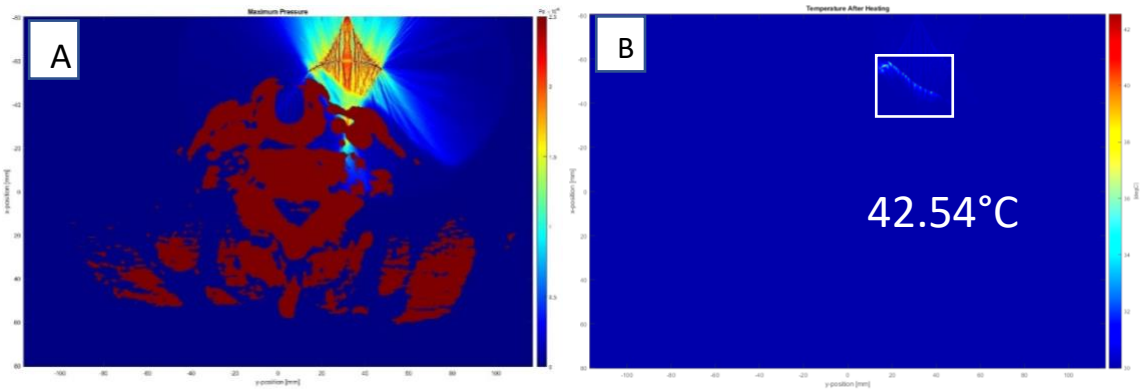

Figure 26: 2-D pressure field simulation of SU-102 through human neck modeling; B: 2-D heat simulation based on simulation results of A.

@3.5MHz, a 3dB decrease in attenuation was achieved by placing H-102 oriented in a lateral to medial orientation rather than a ventral to dorsal orientation in respect to the anterior surface of the cervical neck. Capability of 2-D pressure field simulation with heterogeneous medium enables future optimization of power transfer efficiency. The 2-D simulation results were also important for safety and procedure planning. The script demonstrated here can model any part of the human body given the incorporation of an anatomically correct CT scan. Moreover, patient specific CT scan FUS beam simulation can be carried out prior to FUS-NS therefore providing valuable information on individualized FUS tissue interfaces. In sum, simulation results will help researchers find the perfect position and angle of the transducer to avoid collateral damaged caused to the adjacent tissues and maximize power transfer efficiency.

2-D simulation results of SU-107 show most of the heating occurs at the skin interface. A 10ms burst of 2.5MPa focused ultrasound stimulation causes temperature rise from 30°C to 42.54°C, as shown in Figure 26. This simulation was not applied to A328-Su-F-0.83-IN-PTF since its nominal power is not enough for successful stimulation after attenuation through tissue. Currently, heat simulation could not be applied to H-102 because it requires more computational resource than what's available.

3.1.3 Limitations of KWave simulations:

Although KWave simulator provides great accuracy and powerful built-in functions to help users to build custom simulations, it has unavoidable limitations. The most obvious one is the amount of

resource and time required for the simulations. To satisfy the minimum sampling rate of 2 samples/wavelength (Nyquist rate), the spatial resolution was set to 204 ums. The size of the simulator space needed for both the neck and transducer modeling is 788 by 1144 by 343 grid points. This simulation requires about 150GB of RAM and takes 6 days to complete. The simulation can take approximately 36 hours to run bare minimum simulation with simulation region reduced to only 3cm around the beam. This is due to the complexity of structures. The resources needed drastically decreases for free-field simulations. This constraint demands careful design of simulation models and makes on-the-fly simulations hard to achieve.

There is also a technical and more serious limitation of KWave simulation, which arises from the assumptions KWave makes during its computation. As mentioned in the Methods section, KWave calculates pressure field by solving Equation 5 for each pixel. Equation 5 assumes the background medium is quiescent, which means both net fluid flux and all acoustic parameters of the medium remain the same during the simulation. This is a valid assumption for free field simulation but not for simulations with the human body as medium, within which micro movements of fluid are known to occur. This assumption also became invalid as the acoustic energy increased to a nonlinear domain, where the displacement of the medium caused by the ultrasound beam was too large to be ignored. As mentioned in the Background section, as acoustic power increases, cavities are created in the beam which not only change the geometry of the surrounding medium but also creates bursting pressure field as inertial cavitation forms and collapses. KWave, designed for most diagnostic biomedical ultrasound devices, assumes none of above would be impactful during its computation due to assumed low acoustic power. Therefore, KWave simulation results under high input power may not be fully accurate. Although its low power simulations are relatively more reliable, it suffers from the violation of the assumption of zero net fluid flux through the medium for human body simulations. Following a similar line of logic, the accuracy of 2-D thermal simulation under complex structure is questionable as well. Specifically, the blood flow in the carotid artery near the target region breaks medium's state of quiescence. This explains

the oddity for the demonstrated 2-D thermal simulation result on Figure 26, where all the temperature changes occur at the skin area and no temperature changes at the target.

3.2 System building:

3.2.1 Transducer beam profile measurement:

3.2.1.1 Passive Cavitation Imaging:

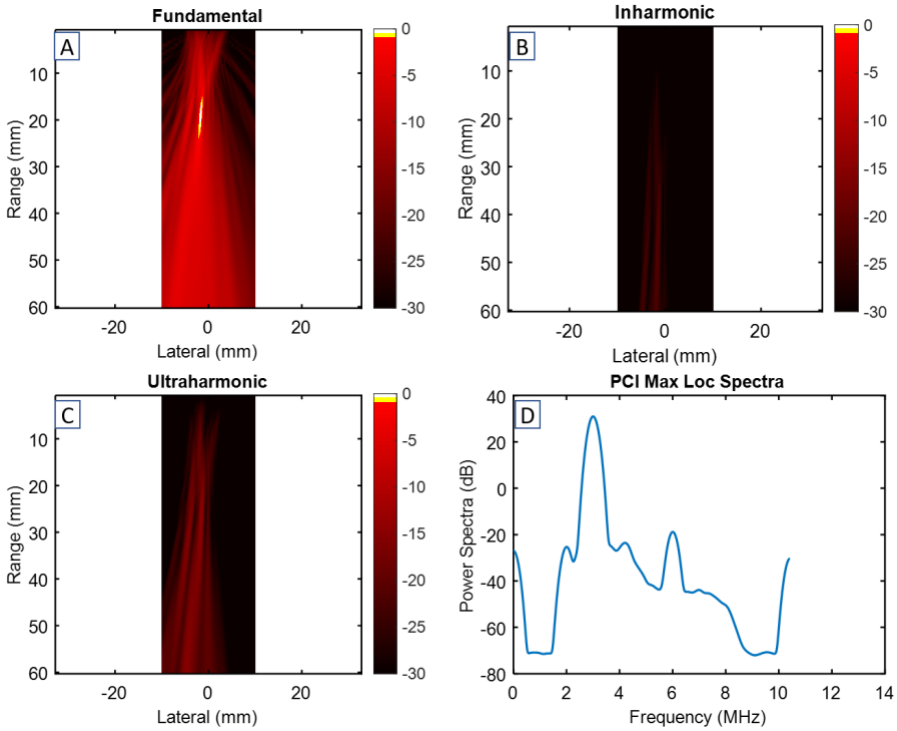

Figure 27: PCI results for SU-107 captured with IP-105 at 5MPa Ppk. Normalized acoustic energy plot at fundamental frequency (A), at inharmonic frequency (B), at ultra-harmonic frequency (C), plot of power spectrum density (D).

As mentioned in the Methods section, the normalized plots at fundamental, inharmonic and ultra-harmonic frequencies provide visualization to the beam profile, stable cavitation and inertial cavitation [29]. With PCI we captured the SU-107 beam profile at is 0.481mm wide and 5.96mm long which match with the simulation results. The Inharmonic plot confirms absence of stable cavitation. The ultra-harmonic plot and absence of broad-band emission on the spectra plot confirm very little inertial cavitation for SU-107 under 5MPa peak positive pressure. This is likely due to low MI of SU-107 under

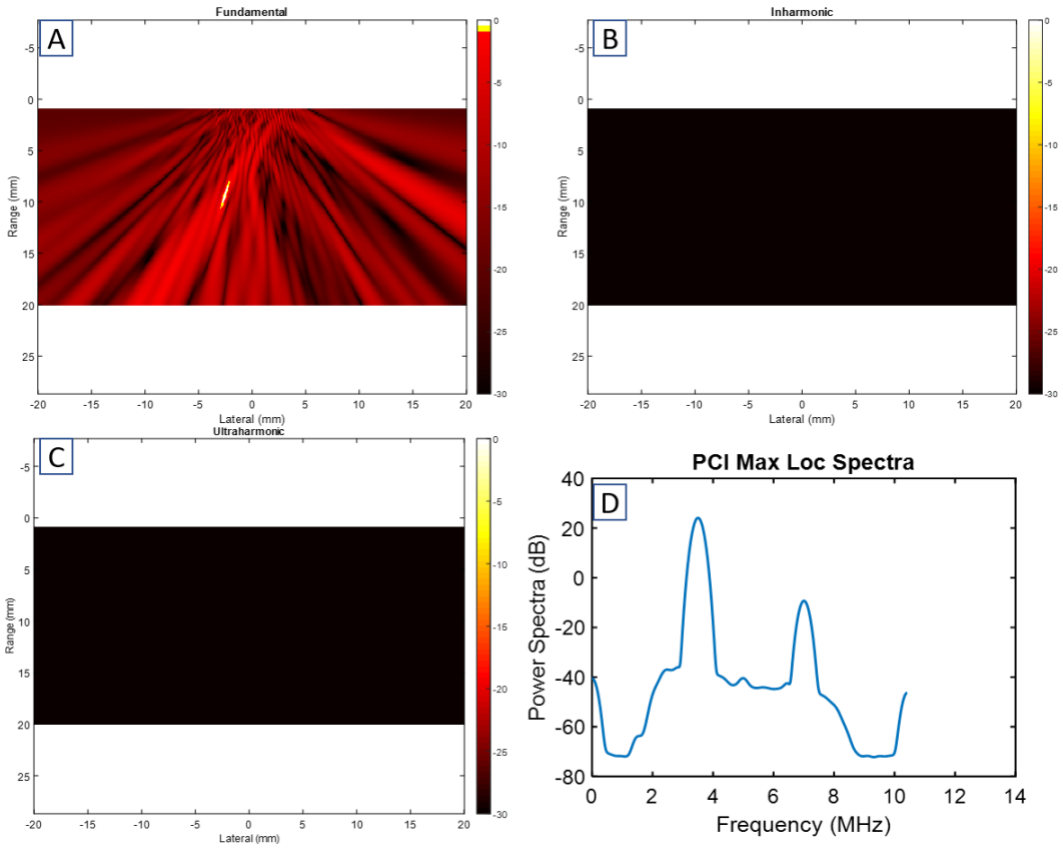

Figure 28: PCI results for A382S-Su-F-0.83-IN-PTF captured with IP-105 at 2MPa Ppk. Normalized acoustic energy plot at fundamental frequency (A), at Inharmonic frequency (B), at ultra-harmonic frequency (C), plot of power spectrum density (D).

5MPa due to its high center frequency. According to Kim et.al, no significant inertial cavitation occurs below 8.17MPa peak negative pressure for a 3.5Mhz transducer [2] .

The PCI results for A382S-Su-F-0.83-IN-PTF shows beam width of 0.26mm and length of 1.9mm, which also matches with the simulation results. The ultra-harmonic and inharmonic plots also confirm absence of cavitation. The spectra plot shows center frequency of A382S-Su-F-0.83-IN-PTF at 3.57MHz.

3.2.1.2 Limitations of Passive Cavitation Imaging (PCI)

Although PCI is a powerful tool to visualize acoustic energy and cavitation profile, it has its limitations. The first constraint is speed of processing. For now, PCI was implemented in MATLAB interfaced to the GTX1070 GPU and is therefore slow. The frame rate when generating Figure 27 was

only 0.25Hz. Therefore, at this current stage PCI can only be used as post-processing instead of real-time analysis. Another limitation is PCI requires the imaging probe to acquire data during the HIFU transducer emission, which Vantage-256 does not support. Vantage-256 uses two separate power supply configurations for HIFU and imaging probes and they must alternately switch back-and-forth to be used in conjunction with each other. Therefore, with our current equipment the PCI cannot be applied to the multi-element HIFU transducer H-102.

3.2.1.2 Test tank scan

As mentioned above, PCI could not be performed on H-102. To obtain its beam profile, H-102 was scanned with HNR-1000 hydrophone inside the AIMS acoustic test tank. Scan results showed the beam to be about 2mm wide and 1cm long, which are with in resolution error to the reported values, as

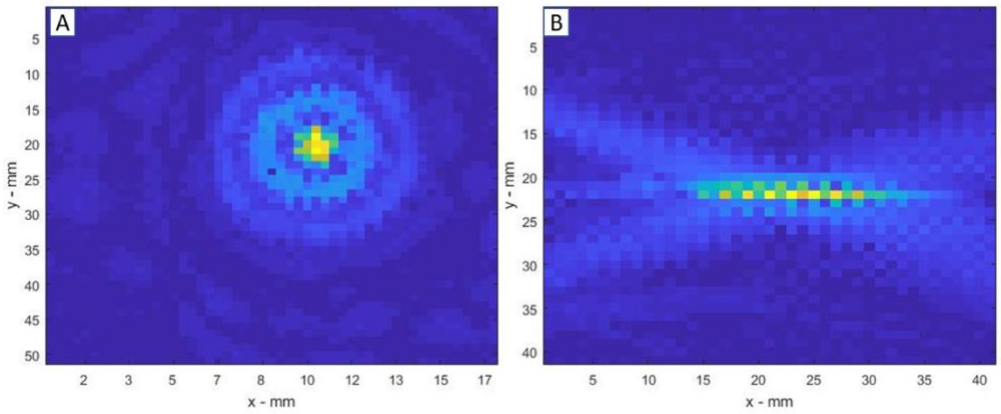

Figure 29: x-y plane scan with 0.3mm step resolution (A); x-z plane scan with 1mm step resolution(B).

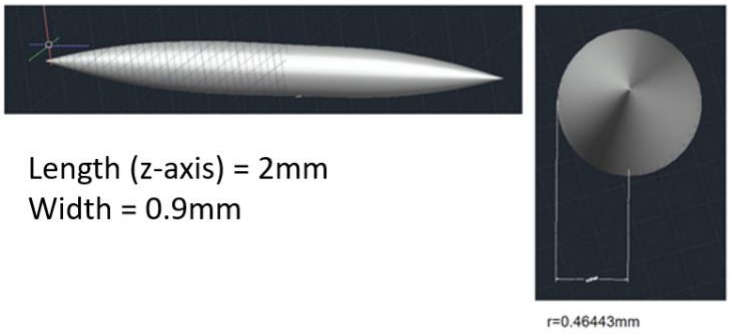

Figure 30: 3-D rendering of a set of x-y plane scan with 0.1mm step resolution of A382S-Su-F-0.83-IN-PTF

shown in Figure 29 and 30. The measured beam dimensions match with both simulated and manufacturer reported values, as shown in Table 1.

3.2.2 Transmit (TX) sub-system:

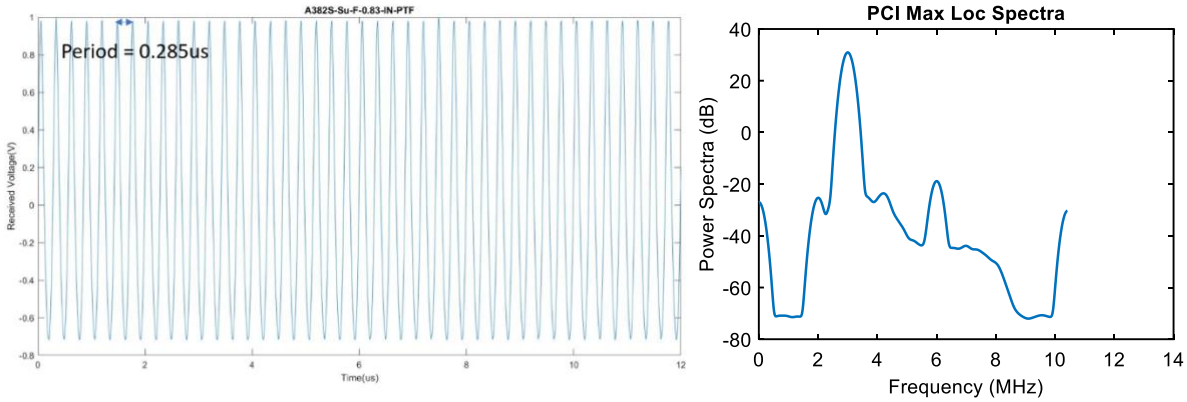

Figure 31: Transmit waveform from AS382S-Su-0.83-IN-PTF with under-sampled input waveform (left), measured with hydrophone; spectra of the transmit waveform from AS382S-Su-0.83-IN-PTF, measured with imaging probe L12-3V. Spectra calculated with PCI.

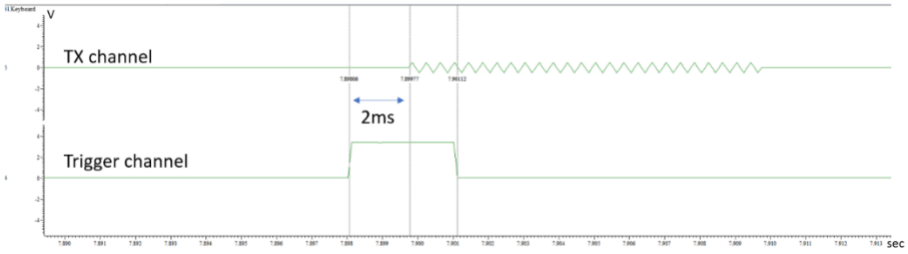

Figure 32: Trigger channel signal and acoustic waveform received by CED1401.

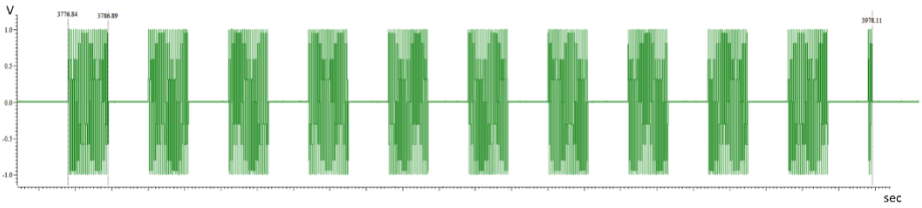

Figure 33: 50Hz, 50% duty cycle, square wave amplitude modulated sinewave produced by custom-built LabVIEW program and VirtualBench digital function generator.

As mentioned in the Methods section, the waveform created by the custom-built LabVIEW program was under-sampled. The transducers were used as bandpass filter to reduce the aliasing noise. To validate, the waveform at 3.57MHz was created by the TX sub-system and scanned by hydrophone HNR-1000. The received waveform has frequency 3.57MHz, shown in Figure 31, which is same as the one

created by TX sub-system. As mentioned in section 2.2, I used the single-element transducer as bandpass filter to suppress the harmonics caused by digitization of waveform from the function generator. Spectra in Figure 31 demonstrates successful suppression of harmonics. Trigger signal was tested with the RX sub-system. Output of the VirtualBench digital function generator was connected to the input of CED1401. Both generated acoustic waveform and trigger signal were visualized with CED software Spike2 (Cambridge Electronics Design Limited, 139 Cambridge Road, Milton, Cambridge BC24 6AZ, England).

The trigger signal is a 3ms long square pulse with a 2ms lead time, as shown in Figure 32. The CED system was triggered with the rising edge of the trigger signal. Modulation capability was tested also with the RX sub-system. A 50Hz, 50% duty cycle, square wave amplitude modulated 3.5MHz sinewave was produced by the TX sub-system and picked up by the CED1401, shown in Figure 33. Pulse width was measured with cursor to be 10.05ms, with a rest period of 10ms. This shows capability of TX sub-system at producing square wave modulated signal.

3.2.3 RX sub-system

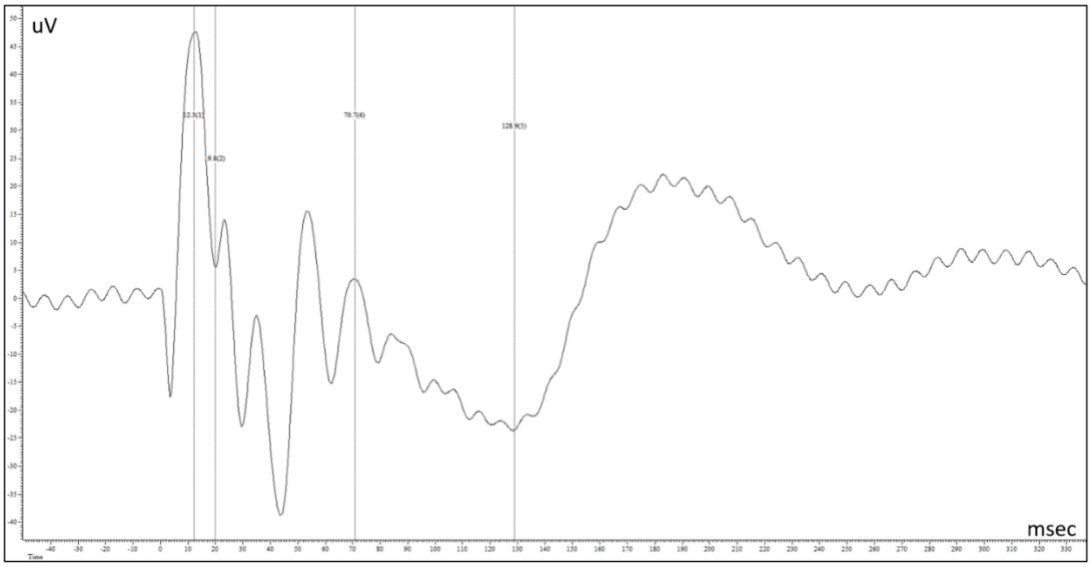

Figure 34: Recorded single-epoch EEG data from Lu with 0.1Hz, 70Vp electrical stimulus applied to his wrist.

RX sub-system, including the CED1902 and 1401 EEG acquisition systems, were connected to C3 at on the scalp with electrical stimulus generated by BIOPAC module STM100C module applied to

the left wrist. The filter on CED systems were set to bandpass at 5-100Hz [34]. The location of C3 on the subject's scalp was determined by the international 10-20 system. The electrical stimulus was a 70Vp pulse at 0.1Hz applied to the median nerve, volar surface of the wrist. Large voltage 70Vp was necessary to ensure electrical pain stimulus (due to A-delta and C fibers) while touch A-beta EP (N20, P70) were filtered. Using this RX system, we were able to measure an electrical and then FUS-NS evoked potential from the somatosensory cortex, as shown in Figure 35. In the recorded EEG data, all the signature peaks of somatosensory evoked potential (SEP) were recognized, including P14, N20, P70 and N100. This successful result demonstrate capability of the CED system at acquiring and filtering EEG data.

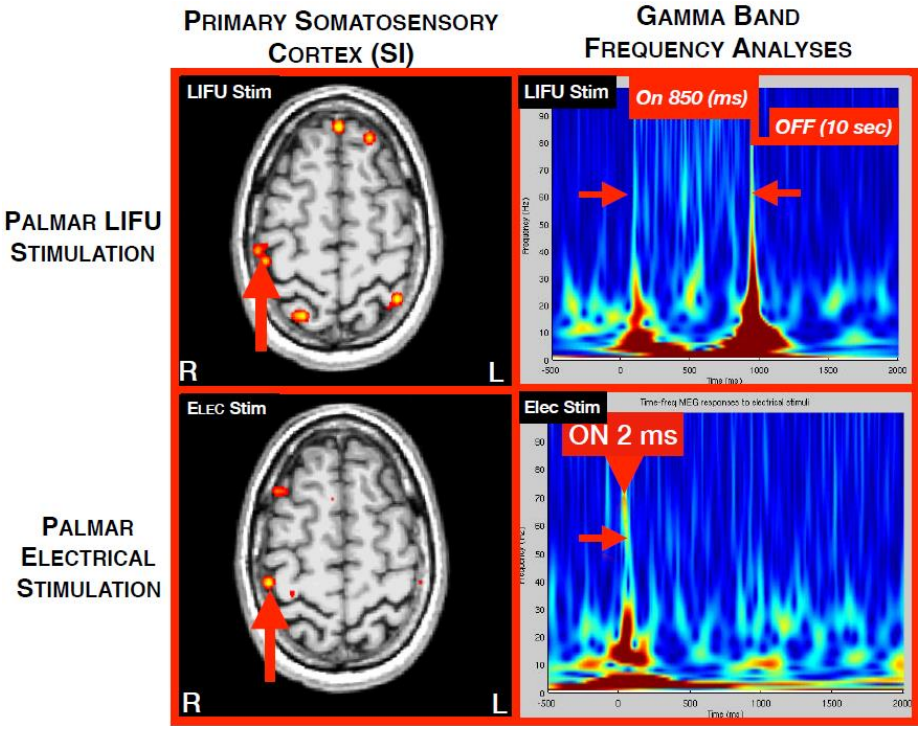

Figure 35: Results of MEG scan of Dr. Lerman's brain during LiFU stimulus (top) and reference electrical stimulus (bottom).

3.3 System Integration and Characterization

3.3.1 The focused ultrasound system (TX + RX sub-systems)

To combine the TX-RX focused ultrasound system we validated each of the individual sub-systems. To ensure safety, A328-Su-F-0.83-IN-PTF was used for all the human subject test. In human testing was approved by UCSD IRB application. The A328-Su-F-0.83-IN-PTF is limited to maximum

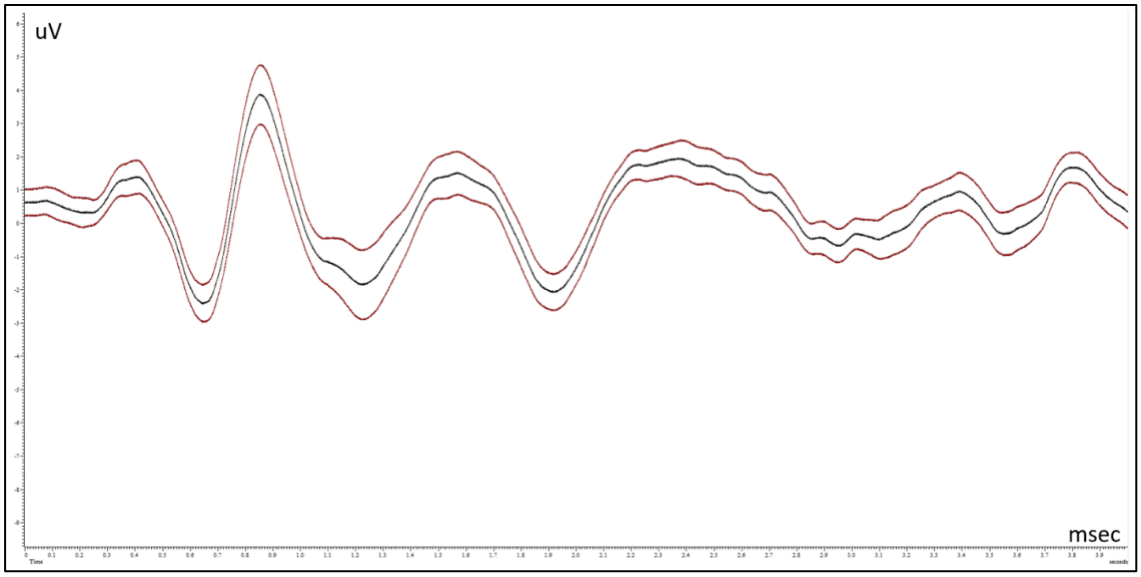

Figure 36: Averaged EEG data from FUS-NS stimulation.

2MPa at its nominal power, which is both mechanically and thermally safe for continuous emission under 1sec as shown in the simulations. Palmer area was chosen as target for this initial test as the branches of median nerve innervates this dermal area of the palm. It was subsequently determined that aiming the beam at the target was very challenging as the acoustic beam was invisible without real-time beam characterization. With stimulus the subjects reported pin prick focal local pain sensation that resembled a bee-sting-like sensation, however only lasting 500 ms. Pain evoked potentials were captured with the CED Micro 1401 Rx system shown in Figure 36.

In addition to obtaining SSEP FUS-NS test was carried out one subject, inside MEG to source localize the FUS-NS pain evoked sensation. 70Vpk electrical stimulus was applied to the subjects left palmar area as reference. Similar sting-like sensation was reported by the subject with both high voltage and the FUS-NS. The results show both FUS-NS and electrical stimulated evoked potential originated from somatosensory cortex. Our data demonstrate efficacy in the pain mediated FUS-NS system and lead to the hypothesis that the pain mediated sensation from FUS-NS was caused by mechanical rather than

thermal energy. To further pursue this hypothesis, we enrolled N=3 human subjects to replicate these findings with a larger cohort.

3.3.2 Human subject study based on custom-built focused ultrasound system

3.3.2.1 Methods:

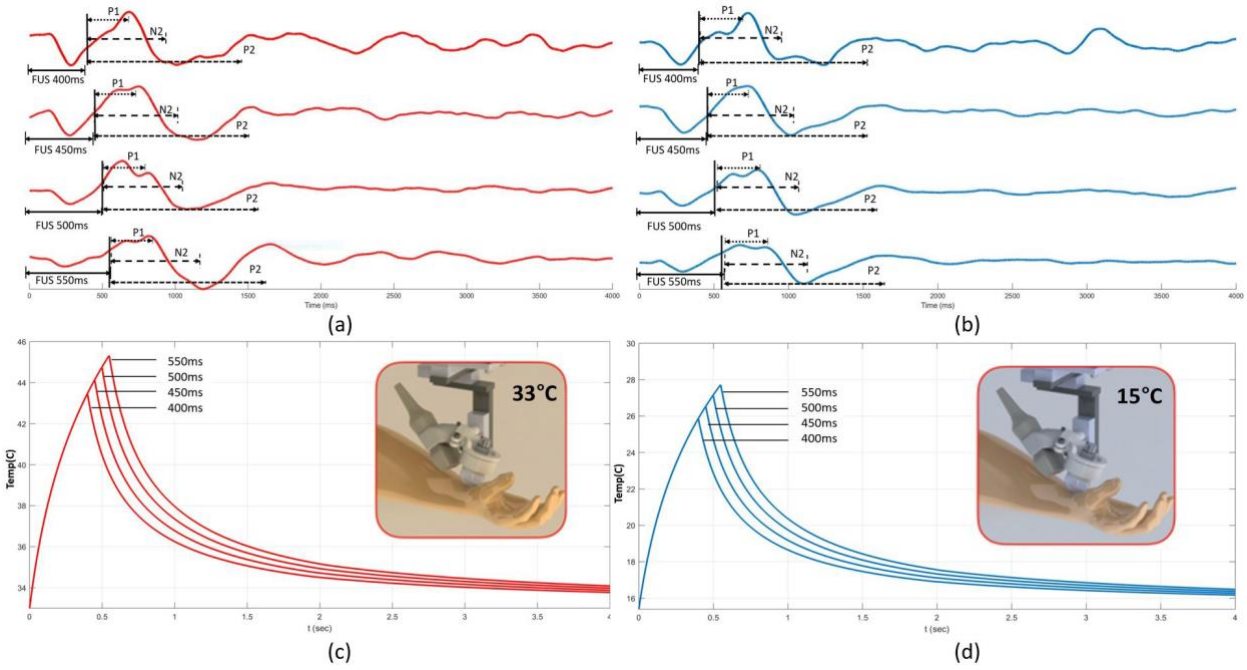

Figure 37: Stacked USEP data with FUS on time=400, 450, 500, 550 ms under (a) warm-hand and (b) cold-hand regime. Heat simulation results from HIFU for subdermal tissue under both regimes: (c) baseline temperature for warm hand is 33C°, and destination temperature

It is known that thermal mediated pain sensation does not occur until a temperature of approximately 43°C is reached [35]. The HIFU heat simulator to was used to estimate increases in subdermal tissue temperature incurred by FUS-NS at ambient temperatures(33°C) and with cooled skin(15.4°C). At ambient temperature 33°C and pulse duration from 400 and 450msec HIFU simulation demonstrate, temperature increase from 33°C (base temperature) to 44.5°C, while pulse duration ranging (500 and 550msec) increase from 33°C to 46.5°C (Figure 37). Based on external skin surface and subdermal human skin temperature provided by ice cooling to subdermal skin tissue temperature predicted to be 15.4°C with endogenous subdermal tissue warming [32]. HIFU heat simulation from ice cooled base temperature (subdermal tissue) = 15.4°C, demonstrate that with 550 ms pulse duration; subdermal tissue

temperature rose to 29°C. Of note at 29°C heat mediated evoked potential responses do not occur [36]. Therefore, we postulated that the FUS-NS sensation which persisted at low temperature (15.4°C increase up to 29°C) confirms that this sensation was caused by mechanical agents and is less likely due to heat.

We carried out a small N=3 Institutional Review Board at UC San Diego (#171154) approved study. Three healthy human subjects (2 females, 1 male; age range 23-29), were recruited. All subjects were deemed healthy by medical and physical examination, did not take any chronic medications, and did not drink alcoholic or caffeinated beverages within 2 days prior to enrollment and throughout the the study week. Subjects underwent two study visits separated by one week. On Visit Day #1 subjects first underwent left wrist electrical stimulation followed by ambient temperature FUS left hand neurostimulation. On Visit Day #2 subjects underwent ice-cooled temperature FUS left hand neurostimulation. An Olympus transducer A382S-Su-F-0.83-IN-PTF (Olympus Scientific Solution Inc., Waltham Massachusetts, US) was used to deliver focused ultrasound pulses with a peak pressure 1.85MPa (Ppk) and acoustic center frequency of 3.5 MHz (fc). The transducer was driven by a 2100L RF power amplifier (ENI Inc., Rochester, New York, US) and programmable waveform generator Virtualbench (National Inst. Austin, TX) under control by a custom-built LabVIEW program. The transducer focal spot is measured as 2 mm by 1 mm, located 0.83 inch away from transducer front face in water. The electrical excitation waveform applied to the transducer via the power amplifier, was a pulsed continuous wave (pulsed-CW). The pulse trains ranged from 400 to 550 msec, followed by a 10 sec rest inter-pulse interveal period i.e., before the next pulse. To sync evoked potential measurements, a trigger signal (TTL pulse) was supplied to the data acquisition system at the start of each pulse. The transducer was mounted on a 3-axis positioning system with 0.1mm accuracy for fine-tuning of focal point position 0.5mm below the dermis. A custom waveguide was built that allowed immersion of the transducer in degassed water and movement within the z axis. Peripheral ultrasound neurostimulation was performed on the left-hand palmar area located between the thenar eminence and base of the index finger. The EEG data acquired were acquired and processed with RX sub-system mentioned in previous sections during

both FUS and electrical stimulation. Epochs were marked via attenuated TTL detection. The MICRO 1401 and Spike2 system acquired TTL initiated a 4-sec-long epoch recording that was subsequently averaged. During FUS stimulation collection USEP peak amplitude and latency data from all subjects (N=3) was collected and labelled P1, N2 and P2. We compared the kinetics of P1, N2, P2 from the acquired USEP with our measured somatosensory evoked potential (SSEP) elicited by electrical stimulation. As we measure only pain evoked potential with the FUS-NS Ultrasound Somatosensory Evoked Potential (USEP) we compared our wave form characteristics (latency, amplitude) to known painful contact heat evoked potential (CHEP) and laser evoked potential (LEP) applied to the median nerve [36] [37] [38]. All the latencies reported in this study are post-stimulus (after offset of FUS). Received EEG data was filtered by a 1-2 Hz bandpass filter to eliminate artifact noise and subsequent large fiber SSEP peaks such as N20 and P70, were also filtered out.

3.3.2.2 Results:

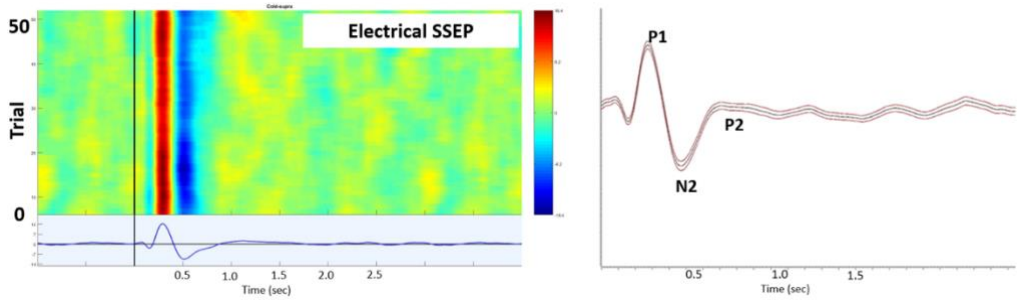

Figure 38: (a) ERP plot for SEP by median electrical stimulation on wrist area; (b) Average SEP by median electrical stimulation on wrist area with standard error mean (red contours).

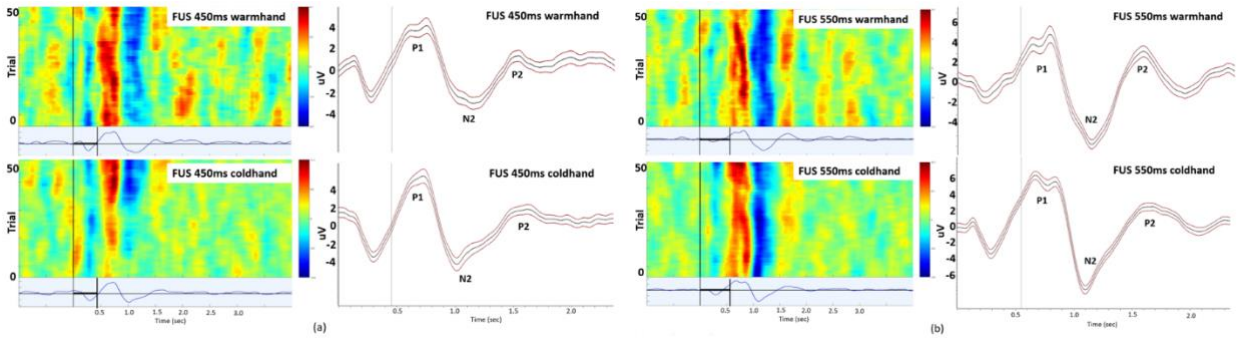

Figure 39: Evoked potential and characteristic peaks under FUS stimulus, with both warm-hand and cold-hand regime. (a) FUS 450ms stimulation, and (b) FUS 550ms stimulation.

At both ambient room (warm-hand=33°C) and with ice cooled (cold-hand=15.4°C) subdermal skin temperatures (we observe a 281 – 350msec post stimulus peak latency of USEP-P1 (the first

Table 2: Amplitude analysis for P1 and N1 in uV

	P1(uV)			N2(uV)		
	cold	warm	p-value	cold	warm	p-value
400ms	5.47 ± 0.37	5.6 ± 0.41	0.841	-5.46 ± 0.34	-6.31 ± 0.55	0.194
450ms	6.14 ± 0.44	6.62 ± 0.54	0.477	-6.00 ± 0.44	-6.22 ± 0.63	0.814
500ms	6.64 ± 0.38	7.07 ± 0.41	0.815	-5.43 ± 0.34	-6.38 ± 0.36	0.572
550ms	6.78 ± 0.33	7.62 ± 0.46	0.232	-5.77 ± 0.39	-6.66 ± 0.45	0.487

Table 3: Latency analysis for P1, N2 and P2 in ms

	cold	warm	p-value	cold	warm	p-value	cold	warm	p-value
400ms	281.20 ± 19.08	316.89 ± 15.37	0.361	663.21 ± 26.82	691.86 ± 23.59	0.402	1014.93 ± 22.11	977.20 ± 25.70	0.469
450ms	277.72 ± 15.86	299.43 ± 15.72	0.605	630.91 ± 30.65	674.99 ± 27.34	0.457	941.23 ± 25.49	1044.86 ± 27.12	0.331
500ms	350.83 ± 17.44	326.87 ± 12.65	0.355	778.86 ± 19.85	725.27 ± 19.14	0.736	1111.05 ± 25.74	1006.34 ± 18.82	0.320
550ms	303.10 ± 12.38	334.17 ± 12.53	0.626	601.47 ± 15.55	739.58 ± 15.94	-	994.15 ± 19.75	1038.59 ± 20.91	0.677

quantifiable evoked potential peak). This latency range matches reported value for median nerve painful CHEP-P1, late potential (LP) of LEP, (approximately 300-400msec) [36] [37] [38], and our own measures of electrical painful SEP (approximately 319.6msec ± 3.5msec for warm-hand and 311.1msec ± 3.5msec for cold-hand). Moreover, the estimated conduction velocity based on measured USEP-P1 ranges from 7.24 to 11.4 m/s and matches reported Aδ fiber conduction velocity, 6.7 - 14.5m/s [39] [40] [41]. The USEP-N2, latency ranged from 586 – 825msec for both cold and warm-hand regimes, matching N2 ULP in LEP at approximately 800msec [38] [39]. The USEPP2, was measured at a latency range 977 – 1044.86msec. This latency range also matches with reported ULP obtained with LEP, ranging from 996 to 1000msec [38] [39]. The estimated conduction velocity of USEP-P2 is approximately 1m/s, also matching reported C-type fiber conduction velocity of 1m/s [41]. We observed similar kinetics (latency and amplitude) of P1, N2, P2 between cold and warm-hand regime($p>.05$) for all four-pulse duration on times measured (400ms, 450ms, 500ms, 550ms).

The above P1, N2, P2 latencies were measured from the FUS offset to peak. All temperature simulations of FUS used in this study demonstrate identical slope temperature rise (Figure 37). If accumulated temperature (heat) was the main contributor to USEP generation (due to activation of thermal nociceptors resulting in pain) the post-stimulus latencies (from FUS offset to peak) of P1, N2, P2 would decrease with longer on times (staying in sync with the heat threshold temperature). In aggregate, (when using a linear mixed effects model), we do not observe a significant decrease($p>.05$) in USEP

latency in either ambient or cold hand temperatures across pulse duration on-times (400, 450, 500, 550 ms) suggesting the absence of a FUS mediated temperature threshold that may elicit thermal nociceptor activation.

Chapter3, section 3.3, in part, has been submitted for publication of the material as it may appear in *Measurement of Focused Ultrasound Neural Stimulation; Somatosensory Evoked Potential at Two Separate Skin Temperatures* in Proceedings of the IEEE International Ultrasound Symposium, 2018, Lu Xu, Yan Gong, Donald Kimball, Rahul Singh, Kristen Nguyen, Ramesh Rao, Mingxiong Huang and Imanuel Lerman. The thesis author was the first author of the paper.

3.3.2.3 Limitations of the above study:

There are a few limitations of this human subject study. First, the subdermal temperature was simulated and estimated based on modeling instead of actual measurement. The actual subdermal tissue temperatures under ultrasound emission during both cold and warm hand period were unknown. Second, the pain like sensation was only achieved with ultrasound beam targeted at branches of free nerve endings underneath skin. The same sensation was not achieved with ultrasound targeted at deeper nerve tissues. This could potentially mean long duration low intensity ultrasound neural stimulation only works for subcutaneous free nerve endings, where many mechanoreceptors and nociceptors reside. Lastly, the implicit assumption made during analysis of evoked potential is that the scalp location and underlying cerebral structures are consistently correlated [42], which might not necessarily be true [43], therefore interindividual variability may contribute.

3.4 Future work: Integrated miniaturized circuit board

As mentioned in the previous sections, real-time PCI requires a separate system to drive the multi-element HIFU transducer H-102. Current efforts are undeway to build real time PCI and eventual harmomnic motion imaging systems. A prototyped single-channel ultrasound TX unit integrated into a printed circuit board was made. The integrated TX unit uses NUCLEO F429ZI development board to replace the arbitrary function generator and trigger generator in the bench-top version to improve

portability and accessibility of the TX unit. This design utilize the clock inside of the NUCLEO F429ZI board, which runs at 180MHz. Two GPIO ports were associated with two timers, which copied this clock. One GPIO was used to output squarewave at a center frequency of the paired transducer and the other used to gate the first GPIO port to create amplitude modulation. The GPIO ports can undersample the CPU clock in a user definable way such that they could output squarewaves with any frequency lower than 180MHz. Then the gated squarewave was bandpass filtered at its fundamental frequency to generate the amplitude modulated sinewave.

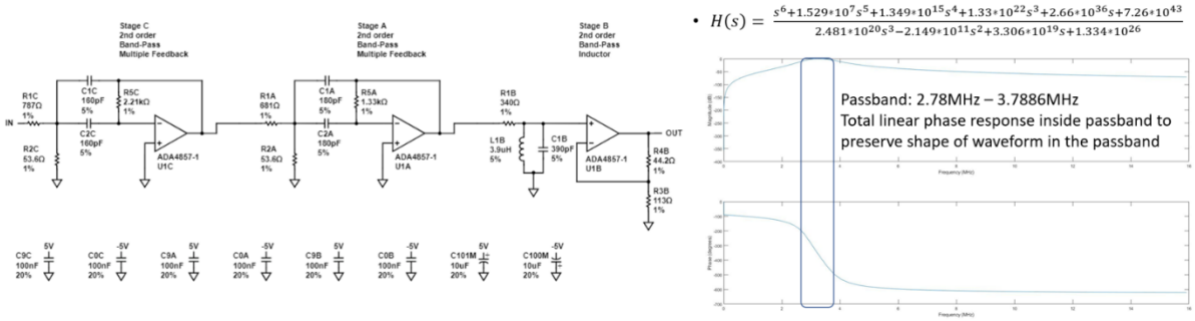

Figure 40: 6-pole bandpass filter implementation in Filter Wizard(left) and design in MATLAB (right)

The bandpass filter was implemented using Filter Wizard (Analog Devices, Inc., Norwood, MA) online filter design toolbox and designed with MATLAB. Passband was chosen as 3.57MHz to fit single element transducer SU-107 and A328-Su-F-0.83-IN-PTF. The high pass threshold at 2.78MHz filters out the DC offset on the modulated square wave while the low pass threshold at 3.7886MHz filters square waves into sinewaves. The circuit was simulated in LtSPICE (Analog Devices, Inc., Norwood, MA) and is currently being manufactured. Once manufactured and tested, this single-channel integrated TX unit can be multiplied to a 64 channel TX system to drive H-102 externally, enabling real-time PCI.

Chapter3, section 3.3, in part, has been submitted for publication of the material as it may appear in *Measurement of Focused Ultrasound Neural Stimulation; Somatosensory Evoked Potential at Two Separate Skin Temperatures* in Proceedings of the IEEE International Ultrasound Symposium, 2018, Lu

Xu, Yan Gong, Donald Kimball, Rahul Singh, Kristen Nguyen, Ramesh Rao, Mingxiong Huang and Imaneul Lerman. The thesis author was the primary investigator and author of the paper.

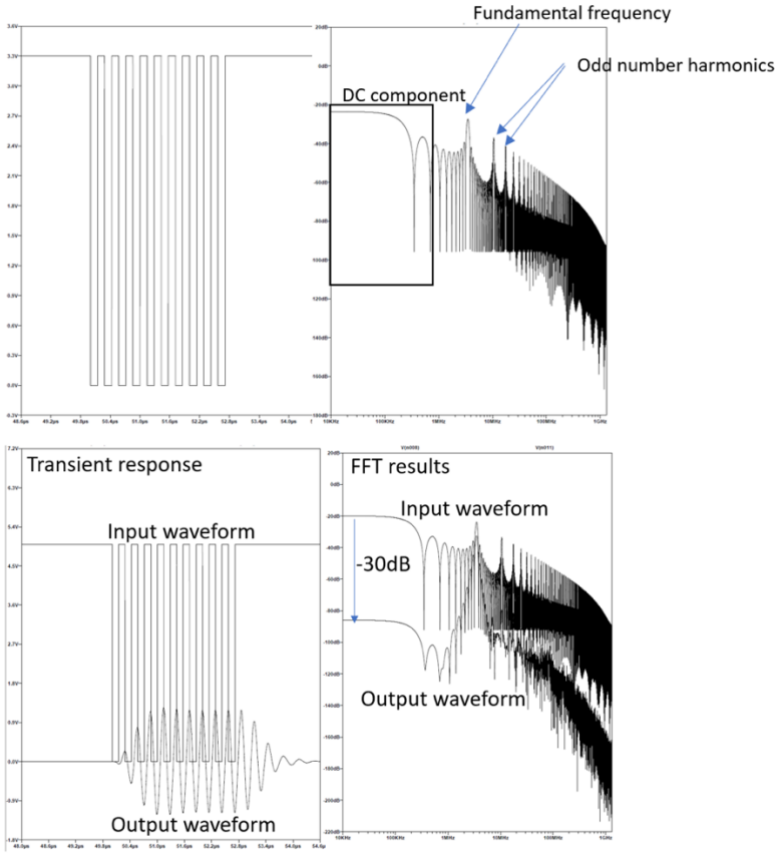

Figure 41: Simulated results in temporal domain(left) and frequency domain(right) with LtSPICE.

Chapter 4. Conclusion:

This study presents design, validation and initial human trial results of a focused ultrasound system specialized in neural stimulation research. This system can produce user definable amplitude modulated pulses, simultaneously acquire and analyze the event-based EEG data. All the individual parts within the system were carefully characterized with simulation and experimentally tested with the focus on optimization of safety parameters. A human subject test (N=3) was carried out with the combined system to demonstrate feasibility of focused ultrasound neural stimulation at palmar area and showed that mechanical energy and not heat contribute to palmar nociception. Focused ultrasound transducers H-102, SU-107 and A328-Su-F-0.83-IN-PTF were characterized using 1-D and 2-D hydrophone scanning, passive cavitation imaging (PCI) and pressure simulations using HIFU simulator and KWave. In sum or pilot work provide a comprehensive TX-RX FUS-NS system that will facilitate research in the mechanism of ultrasound neural stimulation and its therapeutic applications.

References

[1] T. D. Kozai, N. B. Langhals, P. R. Patel, X. Deng, H. Zhang, K. L. Smith, J. Lahann, N. A. Kotov and D. R. Kipke, "Ultrasmall implantable composite microelectrodes with bioactive surfaces for chronic neural interfaces," *Nature Materials,* vol. 11, p. pages 1065–1073, 2012.

[2] M. G. Kim, S. A. Lee, H. A. S. Kamimura and E. E. Konofagou, "Inhibitory effects of motor neuron activity in mouse peripheral nerve system using ultrasound-guided focused ultrasound in vivo," Kobe, Japan, 2018.

[3] L. E. Kinsler and A. R. Frey, Fundamentals of Acoustics, 2nd ed., New York: John Wiley & Sons, 1950.

[4] C. C.Church and E. L.Carstensen, " "Stable" inertial cavitation," *Ultrasound in medicine & biology,* pp. 1435-1437, 2001.

[5] T. Y. Wu, N. Guo, C. Y. Teh and J. X. W. Hay, Theory and Fundamentals of Ultrasound, Springer, 2013.

[6] S. Sakai, "Radiation force measurements at a water-air interface.," *Thesis(MS): Univ of Illinois,* 2003.

[7] J. Slifko, "UNDERWATER SHOCK WAVE FREQUENCY SPECTRUM ANALYSIS. I. SIMPLE WAVEFORMS APPROXIMATING MEASURED PRESSURE PULSES IN WATER (No. NOLTR-61-94).," *NAVAL ORDNANCE LAB WHITE OAK MD.,* 1961.

[8] A. D. Legatt and S. R. Benbadis, "General Principles of Somatosensory Evoked Potentials: Overview, Electrical Stimulation Parameters, Recording Parameters," *Medscape,* 2014.

[9] L. Gavrilov, G. Gersuni, O. Ilyinski, E. Tsirulnikov and E. Shchekanov, "A study of reception with the use of focused ultrasound. I. Effects on the skin and deep receptor structures in man," *Brain Res,* vol. 135, p. 265–277, 1977.

[10] L. Gavrilov, G. Gersuni, O. Ilyinski, E. Tsirulnikov and E. Shchekanov, "A study of reception with the use of focused ultrasound. II. Effects on the animal receptor structures," *Brain Res,* vol. 135, p. 279–285, 1977.

[11] L. Gavrilov, E. Tsirulnikov and I. Davies, "Application of focused ultrasound for the stimulation of neural structures," *Ultrasound Med Biol,* vol. 22(2), p. 179–192, 1996.

[12] L. Gavrilov, "Use of focused ultrasound for stimulation of nerve structures," *Ultrasonics,* vol. 22(3), p. 132–138, 1984.

[13] C. Hong, "Reversible nerve conduction block in patients with polyneuropathy after ultrasound thermotherapy at therapeutic dosage.," *Arch Phys Med Rehabil,* vol. 72(2), pp. 132-7, 1991.

[14] J. Foley, J. Little and S. Vaezy, "Image-guided high-intensity focused ultrasound for conduction block of peripheral nerves," *Ann Biomed Eng.,* vol. 35(1), p. 109–119, 2006.

[15] M. E. Downs, S. A. Lee, G. Yang, S. Kim, Q. Wang and E. E. Konofagou, "Non-invasive peripheral nerve stimulation via focused ultrasound in vivo," *Phys. Med. Biol,* vol. 63, 2018.

[16] A. L. Hodgkin and A. F. Huxley, "A quantitative description of membrane current and its application to conduction and excitation in nerve," *The Journal of Physiology,* vol. 117(4), p. 500–544, 1952 .

[17] T. Heimburg and A. D. Jackson, "On soliton propagation in biomembranes and nerves.," *Proceedings of the National Academy of Sciences,* vol. 102, no. 28, pp. 9790-9795, 2005.

[18] M. Nabili, "FDA media," 26 10 2016. [Online]. Available: https://www.fda.gov/media/100797/download. [Accessed 25 5 2019].

[19] Y. S. Kim, H. Rhim, M. J. Choi, H. K. Lim and D. Choi, "High-intensity focused ultrasound therapy: an overview for radiologists," *Korean journal of radiology,* vol. 9, no. 4, pp. 291-302, 2008.

[20] S. Sapareto and W. Dewey, "Thermal dose determination in cancer therapy," *International Journal of Radiation Oncology Biology Physics,* vol. 10, no. 6, pp. 787-800, 1984.

[21] F. Wu, Z. Wang, P. Lu, Z. Xu, W. Chen, H. Zhu and C. Jin, "Activated anti-tumor immunity in cancer patients after high intensity focused ultrasound ablation," *Ultrasound in medicine & biology,* vol. 30(9), pp. 1217-22, 2004.

[22] G. T. Haar and C. Coussios, "High intensity focused ultrasound: Physical principles and devices," *International Journal of Hyperthermia,* vol. 23, no. 2, pp. 89-104, 2009.

[23] G. T. Haar and C. Coussios, "High Intensity Focused ultrasound: Physical Principles and devices," *Int. J. Hyperthermia,* pp. 89-104, 2007.

[24] B. Treeby, B. Cox and J. Jaros, "k-Wave, A MATLAB toolbox for the time domain, User Manuel," 2016.

[25] F. A. Duck, Physical Properties of Tissue - A comprehensive refence book, San Diego: Academic Press, 1990.

[26] V. Saxena, "Temperature distribution in human skin and subdermal tissues," *Journal of theoretical biology,* pp. 277-286, 1983.

[27] US Food and Drug Administration, "Information for manufacturers seeking marketing clearance of diagnostic ultrasound systems and transducers," Center for Devices and Radiological health, US Food and Drug Administration, Rockville, MD, 1997.

[28] B. C. J. J. Bradley Treeby, "k-Wave - A MATLAB tookbox for the time domain simulation of acoustic wave firlds- user manual," 2016.

[29] K. J. Haworth, K. B. Bader, K. T. Rich, C. K. Holland and T. D. Mast, "Quantitative Frequency-Domain Passive Cavitation Imaging," *IEEE Trans Ultrason Ferroelectr Freq Control,* p. 177–191, 2017.

[30] C. Shannon, "Communication in the Presence of Noise," *Proceedings of the IRE,* pp. 10-21, 1949.

[31] M. A. Wickert, Introduction to Signals and Systems - ECE2610 Lecture Notes, Colorado Springs: Univeristy of Colorado Colorado Springs, 2011.

[32] V. Saxena, "Temperature distribution in human skin and subdermal tissues," *Journal of theoretical biology,* vol. 102(2), pp. 277-286, 1983.

[33] Y. Granovsky, D. Matre, A. Sokolik, J. Lorenz and K. Casey, "Thermoreceptive innervation of human glabrous and hairy skin: a contact," *Pain,* vol. 115(3), pp. 238-247, 2005.

[34] A. D. Legatt and S. R. benbadis, "General Principles of Somatosensory Evoked potentials: Overview, Electrical Stimulation Parameters, Recording Parameters," *Medscape,* 2014.

[35] R. Treede, R. Meyer and J. Campbell, "Myelinated mechanically insensitive afferents from monkey hairy skin: heat-response properties.," *Journal of neurophysiology,* vol. 80(3), pp. 1082-1093, 1998.

[36] Y. Granovsky, D. Matre, A. Sokolik, J. Lorenz and K. Casey, "Thermoreceptive innervation of human glabrous and hairy skin: a contact heat evoked potentials as a valid means to study nociceptive pathways in human subjects," *Neuroscience letters,* vol. 316(2), pp. 79-82, 2001.

[37] A. Chen, D. Niddam and L. Arendt-Nielsen, "Contact heat evoked potentials as a valid means to study nociceptive pathways in human subjects," *Neuroscience letters,* vol. 316(2), pp. 79-82, 2001.

[38] A. Tzabazis, M. Klukinov, S. Crottaz-Herbette, M. Nemenov and D. Yeomans, "Selective nociceptor activation in volunteers by infrared diode laser," *Molecular pain,* vol. 7(1), p. 18, 2011.

[39] D. Bragard, A. Chen and L. Plaghki, "Direct isolation of ultralate late (C-fibre) evoked brain potentials by CO2 laser stimulation of tiny cutaneous surface areas in man," *Neuroscience letters,* vol. 209(2), pp. 81-84, 1996.

[40] R. Kakigi, C. Endo, R. Neshige, Y. Kuroda and H. Shibasaki, "Estimation of conduction velocity of Aδ fibers in humans. Muscle & Nerve," *Official Journal of the American Association of Electrodiagnostic Medicine,* vol. 14(12), pp. 1193-1196, 1991.

[41] W. Magerl, Z. Ali, J. Ellrich, R. Meyer and R. Treede, "C and Aδ-fiber components of heat-evoked cerebral potentials in healthy human subjects," *Pain,* vol. 82(2), pp. 127-137, 1999.

[42] R. W. Homan, J. Herman and P. Purdy, "Experimental Section Cerebral location of international 10-20 system electrode placement," *Electroencephalographv and chmcal Neurophyslology,,* vol. 66, pp. 376-382, 1987.

[43] C. Binnie, E. Dekker, A. Smit and G. Van der Linden, "Practical considerations in the positioning of EEG electrodes," *Electroencephalography and Clinical Neurophysiology,* vol. 53(4), pp. 453-458, 1982.

[44] G. LR, G. GV, I. OB, T. EM and S. EE, "A study of reception with the use of focused ultrasound. I. Effects on the skin and deep receptor structures in man," *Brain Res. ,* vol. 135, p. 265–277, 1977.

[45] Onda Corp., "Onda AIMSIII Datasheet," Onda Corp., Sunnyvale, 2018.

Supplemental File:

Institutional Review Board (IRB) human study application approval letter

UNIVERSITY OF CALIFORNIA, SAN DIEGO
HUMAN RESEARCH PROTECTIONS PROGRAM

Date: April 24, 2018
To: Dr. Imanuel Lerman
Re: Project #171154 The Effects of Transcutaneous Vagus Nerve Stimulation versus Low Intensity Focused Ultrasound Vagus Nerve Stimulation in Healthy Controls Subjects as measured by evoked potential

Dear Dr. Lerman:
Your request submitted March 6, 2018 to amend Project 171154 has been reviewed and approved using the expedited review process based upon your April 12, 2018 response to the Committee's letter to you dated April 11, 2018. This letter verifies that all issues identified in the April 11, 2018 letter have been adequately addressed.

The documents submitted for review on April 12, 2018 included the following: cover letter.
A copy of your revised, approved consent form will be provided to you.

Please note that the amendment approval date does not alter the study expiration date. A modification is given approval only to the expiration date that was received at the most recent initial or continuing review. Also, please check your most recent initial or continuing review approval letter and ensure that continuing review materials are submitted approximately 45 days prior to that expiration.

In addition, IRB amendment approval does not constitute **other institutional required "approvals."** Should your study involve other review entities/committees such as Office of Clinical Trials Administration; Office of Coverage Analysis Administration; Independent Review Committee; Protocol Review Monitoring Committee; committees under Environmental Health & Safety such as Institutional Biosafety Committee and Human Exposure Review Committee; and/or Rady Children's Hospital – San Diego, Research Administration; it is the researchers responsibility to ensure that these entities/committees have been informed of the amendment request, as appropriate.
Thank you for keeping us informed.

On behalf of the UCSD Institutional Review Boards,

/mb

Anthony Magit, M.D.
Director
UCSD Human Research Protections Program
858-246-HRPP (858-246-4777); hrpp@ucsd.edu

cc: CCR

Permission to use AIMS III acoustic tank's schematic from Onda Corp

From: Alfred Yue
Sent: Thursday, May 23, 2019 3:53 PM
To: lux002@ucsd.edu
Cc: py@ondacorp.com
Subject: Web Inquiry

Hi Lu Xu,

Thanks for checking with us. You have our permission to use the schematic/drawing from the User's Manual for your thesis as long as proper citation is given to Onda.

Good luck!

Regards,
Alfred

****
Company: UC San Diego
Name: Lu Xu
Phone: (858) 263-6140
Mobile:
Email: lux002@ucsd.edu
Country: United States
Products: Hyd: 0, AIMSIII: 1, OS: 0, RFB: 0, AQUAS: 0, PCS: 0, Gel: 0, Meas: 0, Cust Dev: 0, Oth: 0, HCT: 0, NPL: 0, CTS: 0
Application: R&D: 0, QC: 0, TQ: 0, PM: 0, Oth: 0, Freq:
Comments: I want to ask permission to use the schematic of AIMS III on its user manual on my thesis.